Plasmodium falciparum diacylglycerol acyltransferase maintains phospholipid homeostasis to regulate sexual differentiation, ER stress, and cytoadhesion

Minako Yoshida[1,2,3], Junpei Fukumoto[4,*], Shinya Miyazaki[5,#], Megumi Tanaka[1,#], Suzumi M. Tokuoka[6,#], Hideru Obinata[7,#], Takaya Sakura[1,2,8], Yoko Onizuka[9], Daniel Ken Inaoka[1,2,8,10], Kiyoshi Kita[2,8,10], Kazuhide Yahata[11], Eizo Takashima[4], Hideo Shindou[12,13], Fuyuki Tokumasu[8,9,*]

[1]Department of Molecular Infection Dynamics, Shionogi Global Infectious Diseases Division, Institute of Tropical Medicine (NEKKEN), Nagasaki University, Nagasaki 852-8523, Japan
[2]Department of Infection Biochemistry, Institute of Tropical Medicine (NEKKEN), Nagasaki University, Nagasaki 852-8523, Japan
[3]Graduate School of Biomedical Sciences, Nagasaki University, Nagasaki 852-8523, Japan
[4]Division of Malaria Research, Proteo-Science Center, Ehime University, Ehime 790-8577, Japan
[5]Department of Protozoology, Institute of Tropical Medicine (NEKKEN), Nagasaki University, Nagasaki 852-8523, Japan
[6]Department of Lipidomics, Graduate School of Medicine, University of Tokyo, Tokyo 113-0033, Japan
[7]Core Facility Management and Technical Collaboration Center, Gunma University, Gunma 371-8511, Japan
[8]School of Tropical Medicine and Global Health, Nagasaki University, Nagasaki 852-8523, Japan
[9]Department of Laboratory Sciences, Graduate School of Health Sciences, Gunma University, Gunma 371-8514, Japan
[10]Department of Biomedical Chemistry, Graduate School of Medicine, The University of Tokyo, Tokyo 113-0033, Japan
[11]Division of Molecular Parasitology, Proteo-Science Center, Ehime University, Ehime 791-0295, Japan
[12] Department of Lipid Life Science, National Institute of Global Health and Medicine, Japan Institute for Health Security, Tokyo 162-8655, Japan
[13]Department of Medical Lipid Science, Graduate School of Medicine, The University of Tokyo, Tokyo 113-8654, Japan

*Corresponding Authors: Junpei Fukumoto, Ph.D.
Division of Malaria Research,
Proteo-Science Center,
Ehime University,
Ehime 790-8577, Japan
TEL: +81-89-927-8277
Email: fukumoto.jumpei.fk@ehime-u.ac.jp

*Corresponding Authors: Fuyuki Tokumasu, Ph.D.
Department of Laboratory Sciences,
Graduate School of Health Sciences,
Gunma University,
Gunma 371-8514, Japan
TEL: +81-27-220-8915

Email: ftokumasu@gunma-u.ac.jp

#Equally contributing authors.

Keywords: *Plasmodium falciparum*; Diacylglycerol acyltransferase; Lipid droplet; Sexual differentiation; ER stress; Cytoadhesion; DiCre recombinase-based conditional knockout

Abstract

Plasmodium falciparum is the causative agent of human malaria, a life-threating infectious disease that imposes a major global health burden. Lipid metabolism is indispensable for this parasite's replication and survival, yet most of the molecular components and mechanisms involved remain poorly understood. In eukaryotes, lipid droplets (LDs) serve as dynamic organelles that store neutral lipids (NLs), buffer lipotoxic stress, and regulate signaling pathways, with their biogenesis controlled by diacylglycerol o-acyltransferases (DGATs). Although *P. falciparum* encodes a putative DGAT (PF3D7_0322300), its role in the parasite life cycle has not been elucidated. We generated conditional PfDGAT-knockout parasites to investigate the enzyme's functional significance. PfDGAT deficiency led to parasite death, accompanied by reduced LD formation, elevated phospholipid levels, and induction of ER stress. Moreover, PfDGAT deletion altered protein trafficking, resulting in the decreased cytoadherence of parasite-infected erythrocytes to human brain microvascular endothelial cells, and suppressed parasite sexual differentiation. Thus, PfDGAT deletion affected multiple aspects of the parasite's life cycle, highlighting its critical role in parasite survival and pathogenesis. Our findings provide new insights into parasite lipid homeostasis and highlight DGAT as a potential target of antimalarial intervention.

Introduction

Malaria parasites invade erythrocytes and undergo exponential proliferation during intraerythrocytic developmental cycles, producing dozens of daughter merozoites within a single round. This proliferative process greatly expands the parasite membrane surface area, necessitating a large supply of phospholipid species. Although the parasites can incorporate certain lipids from the host and external environment, the availability of de novo-synthesized and stored phospholipids is essential for their ability to adapt to rapid fluctuations in lipid content while maintaining an appropriate lipid composition[1-3]. The sexual differentiation of the parasite into the gametocyte stage also requires a characteristic lipid profile. Therefore, lipid synthesis is important for their survival in the bloodstream, subsequent uptake by mosquitos, and adaptation to the new environment within the mosquito[4-6].

The relative composition of lipid species directly determines both the biophysical properties and biological functions of cellular membranes, including the maintenance of membrane integrity, the formation of vesicles and their fusion to a target membrane, and the functional activities of membrane proteins. Lipid species with various acyl chain lengths and head groups have distinct molecular shapes and exhibit different intermolecular interactions, and thereby generate membrane lipid heterogeneities characteristic to specific cell types and organelles. In vesicular protein trafficking, the budding and fusion of small vesicles involve

the formation of an intermediate structure ("hemifusion") characterized by negative membrane curvature[7,8]. To generate and maintain such curvature, phospholipids with small head groups, such as phosphatidylserine (PS), phosphatidylethanolamine (PE), phosphatidic acid, and the more rectangular diacylglycerol (DAG), must be present at defined concentrations to enable efficient hemifusion[9,10]. A comprehensive understanding of the enzymes that synthesize these lipid classes, which are critical determinants of vesicle formation, is crucial, as proper protein trafficking cannot otherwise be explained.

Triacylglycerols (TAGs), a major group of NLs, constitute the core of lipid droplets (LDs), together with cholesteryl esters[11,12]. Although LDs primarily function as reservoirs of NLs, they also protect against lipotoxicity by ameliorating ER stress, serve as principal sites of metabolite flux, act as nutrient sensors through LD-localizing proteins, and form membrane contact sites (MCSs) with other organelles[13]. These functions are essential for maintaining cellular homeostasis[14]. In eukaryotes, TAGs are synthesized in two ways: acyl chain incorporation into DAG from the *de novo* phospholipid synthesis (Kennedy) pathway, catalyzed by diacylglycerol acyltransferase (DGAT), and (acyl-CoA-independent) acyl chain transfer from phospholipids to DAG by phospholipid:diacylglycerol acyltransferase[15]. Mammals possess two DGAT enzymes, DGAT1 and DGAT2, which share no sequence homology but compensate for each other functionally. Both enzymes are localized to the ER,

while DGAT2 is also localized to LDs[16]. DGAT1 has relatively broad substrate specificity, enabling it to act on several substrates[17], whereas DGAT2 functions primarily as the canonical DGAT enzyme catalyzing TAG synthesis. DGAT2-knockout mice exhibit impaired skin barrier function, leading to postnatal death, and display a decrease in carcass TAG levels of up to 90%[18]. By contrast, DGAT1-knockout mice survive, maintain a lean body mass, and are resistant to high-fat-diet-induced obesity[19]. In murine embryonic fibroblasts, DGAT1 deficiency, which impaired TAG synthesis, promotes oleate-induced lipotoxicity[20].

P. falciparum database homology searches have identified a single putative DGAT gene, designated *Pfdgat* (PF3D7_0322300). The PfDGAT protein shares sequence similarity with human DGAT1 at the amino acid level, but not with DGAT2. It has been predicted to be essential based on a double-crossover recombination study and piggyBac genome-wide screening[21,22]. In addition, ghosts of *P. falciparum*-infected erythrocytes, as well as the heterologous expression of PfDGAT in CHO cells, demonstrated diacylglycerol acyltransferase activity, suggesting that PfDGAT may function as a DGAT enzyme in malaria parasites[21,23]. However, the detailed role of PfDGAT in parasite biology remains unexplored.

We therefore generated a conditional PfDGAT-knockout parasite and demonstrated that this enzyme is essential for asexual proliferation. Loss of PfDGAT led to elevated phospholipid levels, which likely suppressed parasite sexual differentiation. In addition, PfDGAT dysfunction triggered ER stress, impaired protein trafficking, and prevented parasite cytoadherence to brain microvascular endothelial cells. The broad impacts of this single-gene knockout highlight the importance of the coordinated maintenance of both glycerol backbones and fatty acid chains in *P. falciparum* biology.

Results

PfDGAT possesses conserved DGAT1 motifs and the membrane bound *O*-acyltransferase motif

The amino acid sequence of PfDGAT was shown to share 24%–30% similarity with DGAT1s from mammals, flies, nematodes, and plants, but no significant similarity to the DGAT2s from these organisms[21]. To assess the spatial similarity between PfDGAT and human DGAT1 (HsDGAT1), we superimposed the predicted three-dimensional conformations (Fig. 1a). Multiple structural regions overlapped between the two proteins, including the FYXDWWN and the SXXXHEY motifs, both of which are highly conserved among DGAT1 enzymes and essential for catalytic function[24,25,26]. By contrast, the N-terminal intrinsically disordered region (IDR) of HsDGAT1 (residues 1–94) had no corresponding region in PfDGAT, which instead possessed its own distinct IDR between residues 158 and 220 (Fig. 1a). The FYXDWWN and SXXXHEY motifs are conserved in DGATs from *Plasmodium* species but absent in those from the other apicomplexan parasites *Toxoplasma gondii* and *Cryptosporidium parvum* (Fig. 1b). This suggests that these organisms either possess unidentified DGAT(s) or their DGATs feature unique catalytic motifs.

DGAT1 is a member of the membrane-bound *O*-acyltransferase (MBOAT) family characterized by distinct sequence motifs[27,28]. In mammals, DGAT1 contains the MBOAT

motif B, characterized by the conserved amino acid sequence "WNI", whereas the other MBOAT motifs (A, C, and D) are not present[27]. PfDGAT was found to possess WNL at the corresponding position (Fig. 1b), suggesting that PfDGAT belongs to the MBOAT family, similar to mammalian DGAT1.

PfDGAT is essential for asexual replication and stage transition in *P. falciparum*

To investigate the physiological roles of PfDGAT, which is predicted to function in the Kennedy pathway (Fig. 2a), we generated conditional knockout parasite lines (*Pfdagt*:LoxPint:HA) with the dimerizable Cre recombinase (DiCre) system (Fig. 2b)[29,30]. We constructed a plasmid to conditionally remove the *Pfdgat* sequences, including regions encoding the FYXDWWN and SXXXHEY motifs, in a rapamycin-dependent manner by flanking them with LoxP sites. The plasmid was incorporated into the parasite genome utilizing the selection-linked integration (SLI) method,[31] and its incorporation was verified by diagnostic PCR (Fig. 2c). To confirm whether the conditional knockout system would function in the established parasite lines, PCR and western blotting were performed (Fig. 2d,e). DNA band shifts were observed in rapamycin-treated *Pfdagt*:LoxPint:HA B10 and G12 clonal lines, which indicated that the *Pfdagt* locus flanked by LoxP sites was excised from the genome (Fig. 2d). Western blot analysis revealed a substantial decrease in PfDGAT expression levels after 24 hours of rapamycin treatment in both clonal lines (Fig. 2e). The

loss of PfDGAT in the two synchronized clonal lines resulted in significantly slower growth from day 6 after rapamycin treatment (Fig. 2f). This demonstrated that *Pfdgat* is essential for parasite growth in the erythrocytic stages, consistent with previous reports[21,22]. The *Pfdgat*:LoxPint:HA B10 clonal line was used for further analyses, as no obvious differences were observed between B10 and G12 clones in terms of gene knockout efficiency or growth kinetics.

To investigate the stage-dependent effect of PfDGAT deficiency, we tightly synchronized parasites within a 0–4 hour window and monitored their growth over time following rapamycin treatment (Fig. 2g–i). At 96 hours post-infection (hpi), slightly condensed and pyknotic parasites were observed in the rapamycin-treated (+Rap) group, and their proportion had increased to approximately 50% by 168 hpi. No obvious shifts in parasite stages were observed, even at 192 hpi, suggesting that *Pfdgat* deletion had negative effects on all parasite stages or no specific stage-dependent effects.

In mammalian cells and yeast, DGAT family proteins localize at the ER membrane. Ectopically expressed PfDGAT was shown to colocalize with ER-resident chaperone proteins calnexin on the ER[1], but it is not clear if PfDGAT naturally localizes at the ER. This encouraged us to investigate the subcellular localization of PfDGAT in *P. falciparum*.

Immunofluorescence assay (IFA) showed that PfDGAT colocalized with the ER-resident chaperone protein BiP on the ER of the parasite throughout the asexual stage (Fig. 2j), indicating that PfDGAT functions at the ER, as seen for the other DGAT family proteins, in processes such as LD biogenesis.

PfDGAT deficiency led to a reduction in NL level and induced ER stress in the parasite

Previous reports have described that erythrocytes parasitized with *P. falciparum* and mammalian cells expressing humanized PfDGAT exhibit DGAT activity, synthesizing TAGs from DAGs[1,21]. To determine whether PfDGAT is functionally involved in TAG synthesis within the parasite, we stained NL-rich compartments, such as LDs, with LipidTOX and monitored NL levels in PfDGAT-deficient parasites at 96, 144, and 192 hpi. As sterol esters are absent in malaria parasites[32], the LipidTOX signal primarily reflects the TAG content. At 96 and 144 hpi, +Rap and rapamycin-untreated (−Rap) parasites showed comparable levels of NL; however, +Rap parasites exhibited a significant reduction in NL levels at 192 hpi (Fig. 3a, b). This suggests that PfDGAT is capable of synthesizing TAG within the parasite during its asexual stage.

Following the decrease in TAG levels in PfDGAT-deficient parasites, available acyl-CoAs are no longer used for TAG synthesis. This shift results in an abnormal phospholipid-to-NL

ratio or a disruption of the equilibrium between free fatty acids (FFA) and acyl-CoAs, ultimately leading to an elevated FFA level in the ER, as reported elsewhere[33] (Fig. S1, S2). This may trigger ER stress, which could ultimately lead to parasite death, as demonstrated by the growth assay (Fig. 2f). To confirm whether ER stress is induced in *Pfdgat*-deleted parasites, we investigated the phosphorylation levels of *Plasmodium falciparum* eukaryotic initiation factor 2α (PfeIF2α), a marker of ER stress[34,35]. At 216 hpi, +Rap parasites showed higher levels of phosphorylated PfeIF2α (P-PfeIF2α) than −Rap (Fig. 3c), suggesting PfDGAT deficiency promoted ER stress in the parasite.

PfDGAT deficiency altered the triacylglycerol and phospholipid profiles in the parasite

To investigate the effect of PfDGAT on triacylglycerol and phospholipid profiles, we performed lipidomic analyses on +Rap and −Rap *Pfdgat*:LoxPint:HA parasites at 78 hpi, a time point when the parasites had not yet shown signs of death or morphological abnormalities (Fig. 2g–i). In +Rap parasites, the fractions of 16 TAG species increased relative to the total TAG content (Fig. 4a–c). These elevated TAG species contained at least one polyunsaturated fatty acid (PUFA), suggesting that PUFAs were less susceptible to hydrolysis than saturated fatty acids in the PfDGAT-deficient parasites, although TAG lipase activity has not yet been characterized in terms of its function and substrate preference. In

contrast, total TAG levels were comparable between +Rap and −Rap parasites at 78 hpi (Fig. S1a), consistent with the NL staining (Fig. 3a, b).

Seven classes of phospholipids were detected in our analysis: lysophosphatidylcholine (LPC), phosphatidylcholine (PC), phosphatidylethanolamine (PE), phosphatidylserine (PS), phosphatidylinositol (PI), and sphingomyelin (SM). We quantified the relative abundance of individual molecular species within each phospholipid class in proportion to the total content of that class, thereby identifying which species were affected by *Pfdgat* deletion. In +Rap parasites, most PC species showed a relative increase (Fig. S1a), except for PC(32:0), PC(34:1), and PC(38:9)/PC(e38:1). PE species containing fatty acids with total carbon numbers of 32 to 34 [PE(32–34:n)] were reduced compared to total PE in +Rap parasites, whereas PE (36–49:n) were elevated (Fig. S1b). In contrast, SM(32-36:n) species increased, while SM(40–44:n) decreased in +Rap parasites (Fig. S1e). The relative abundance of PI and PS species was largely unaffected, although the number of detectable species in these classes was lower than in other phospholipid classes.

Following our investigation of relative abundance, we next examined the total abundance of each lipid class, including TAG. The total abundance of all phospholipid classes was markedly elevated in +Rap parasites, whereas TAG levels remained unchanged (Fig.

S2a–h). These results indicate that PfDGAT deficiency exerts an impact on phospholipid metabolism before influencing TAG.

PfDGAT deficiency abolished gametocytogenesis without effecting gametocyte development

Our previous study demonstrated that NL levels were elevated in *P. falciparum* gametocytes[4]. This prompted us to investigate the physiological function(s) of PfDGAT in the gametocyte. To explore the effect of PfDGAT on gametocyte development, gametocytemia was monitored between days 12 and 15 (mid- to late-gametocytogenesis period) following rapamycin treatment on day 9 (Fig. 5a). Although *Pfdgat* was successfully excised from the genome (Fig. 5b), gametocytemia in +Rap parasites remained comparable to that of −Rap parasites (Fig. 5c). Additionally, no obvious differences in gametocyte stage distribution were observed between +Rap and −Rap parasites (Fig. 5d). This suggests that PfDGAT is dispensable for the maturation of gametocytes.

Given the elevated levels of intracellular LPC and other phospholipids in +Rap parasites (Fig. S2b), we investigated gametocyte conversion in the PfDGAT-deficient parasite, as extracellular LPC is known to suppress this process[36]. Highly synchronized ring-stage parasites were maintained in the presence or absence of rapamycin for 24 hours (Fig. 5e).

Following this treatment, trophozoite- and schizont-stage parasites were collected using magnetic columns, and *Pfdgat* excision was confirmed by diagnostic PCR at day 0 (Fig. 5f). Parasitemia was quantified on day 1, and N-acetylglucosamine (NAG) treatment was initiated and maintained until day 4. From days 5–9, gametocytemia was assessed. We observed that most PfDGAT-deficient parasites failed to develop into gametocytes (Fig. 5g) and that gametocytemia was significantly reduced in +Rap parasites on days 5–9 (Fig. 5h). We quantified the relative expression of AP2-G, a master transcriptional regulator of gametocytogenesis[37,38], but no differences in transcriptional levels were observed on days 0 and 1 in our quantitative reverse transcription PCR (qRT-PCR) analysis (Fig S3).

PfDGAT deficiency impaired cytoadhesion of parasites to human brain endothelial cells

Cerebral malaria is primarily attributed to the cytoadherence of parasite-infected erythrocytes to endothelial cells lining the brain microvasculature, a process mediated by the transport of *Plasmodium falciparum* erythrocyte membrane protein 1 (PfEMP1)—a family of adhesive proteins encoded by approximately 60 *var* genes[39]—to the surface of the infected erythrocyte membrane. Given that ER stress has been shown to impair protein trafficking, we investigated the potential role of PfDGAT in parasite adhesion to human brain microvascular endothelial cells (HBMECs). We evaluated the ability of PfDGAT-deficient

parasites to adhere to HBMECs under both static and flow conditions (Fig. 6a). +Rap and −Rap parasites were maintained from days 1–6, followed by sorbitol treatment for ring-stage synchronization. Subsequently, one of the two −Rap groups was treated with brefeldin A (BFA), a protein-trafficking inhibitor, to serve as a negative control for cytoadhesion[40,41]. After 18 hours of the treatment, the parasites were transferred either to culture dishes or microfluidic chambers containing cultivated HBMECs. In both conditions, +Rap parasites exhibited significantly reduced cytoadhesion than −Rap, with levels comparable to those of BFA-treated parasites (Fig. 6b, c). This suggests that PfDGAT is involved in parasite cytoadhesion to HBMECs. To elucidate the underlying mechanism responsible for the low cytoadhesive ability of PfDGAT-deficient parasites, protein trafficking was observed in +Rap and −Rap parasites by analyzing the localization of skeleton binding protein 1 (SBP1), a protein exported to Maurer's clefts[42], using IFA (Fig. 6d). On days 6 and 8, SBP1 abundance was significantly reduced in PfDGAT-deficient parasites, indicating that PfDGAT plays a potential role in protein trafficking and influences the parasite's cytoadhesive propensity, possibly through altered PfEXP1 exposure.

Discussion

Although PfDGAT has been implicated in LD biogenesis, its biological functions in malaria parasites remain largely uncharacterized. Because the parasite is thought to lack β-oxidation activity[43,44], which converts the fatty acids released from TAGs into energy sources, it remains unclear how TAGs stored in LDs through PfDGAT activity contribute to the parasite life cycle. In this study, we demonstrated that PfDGAT deficiency results in parasite death, completely blocks sexual differentiation, and severely impairs the cytoadhesive ability of the parasite (Fig. 2e–h, Fig. 5g, h, and Fig. 6b, c), underscoring the pivotal role of this enzyme in the malaria parasite life cycle.

PfDGAT has the potential to become a highly promising drug target in malaria parasites because PfDGAT deficiency adversely affects various aspects of the parasite's life cycle, as shown in this study. However, a comparative analysis of the amino acid sequences and superimposed structures of PfDGAT and HsDGAT demonstrated that their catalytic motifs and spatial arrangements are similar (Fig. 1a,b). These findings indicate that their substrate preferences and catalytic specificities are likely comparable, suggesting that inhibitors targeting these enzymatic sites would be effective against both enzymes. Indeed, treatment with T863, a selective HsDGAT1 inhibitor targeting the acyl-CoA-binding pocket[45], resulted in decreased lipid formation and growth arrest in *P. falciparum*[46], although it remains unclear

whether T863 specifically targets PfDGAT. A recent study showed that the N-terminal IDR of HsDGAT1 is essential for dimerization and DGAT activity[25]. While PfDGAT does not possess an discernable IDR at the N-terminus, such a region is predicted to reside between amino acid residues 158 and 220 (Fig. 1a). Although dimerization of PfDGAT was not detected by western blotting under reducing conditions, this IDR may nevertheless play a crucial role in intermolecular interactions and enzymatic activity within the parasite, suggesting that this region could serve as a potential target for PfDGAT-specific drug development.

PfDGAT deficiency probably led to elevated FFAs in the parasite. As excess FFAs cannot be incorporated into DAG in the form of acyl-CoA, this ultimately resulted in reduced TAG levels and fewer LDs (Fig. 3a,b). FFAs are normally either degraded as energy sources via β-oxidation, which is likely inactive in the malaria parasite, or used for phospholipid synthesis as components of the cellular membrane. In PfDGAT-deficient parasites, increased phospholipid levels suggest that the acyl-CoAs not incorporated into DAG are diverted to phospholipid synthesis (Fig. S2). We reasoned that the parasite senses elevated levels of phospholipids, particularly LPC, as a signal of a replication-favorable environment, and thus halts its sexual differentiation, even under gametocytogenesis-inducing conditions (Fig. 5g, h). Excess FFAs have been demonstrated to trigger ER stress[47-49], as was also

observed in PfDGAT-deficient parasites (Fig. 3c). ER stress also elicits adaptive responses, such as the unfolded protein response, which is mediated by the membrane perturbation sensors IRE1 and PERK[50] and serves to alleviate stress. Because phospholipid levels have been shown to increase under ER stress[51-53], the increased levels of phospholipid observed in PfDGAT-deficient parasites may reflect not only a diversion of metabolic flux but also a parasite response to ER stress. However, prolonged ER stress ultimately leads to parasite death in PfDGAT-deficient parasites (Fig. 2e–h), as reported previously[54].

PfDGAT-deficient parasites showed reduced binding to HBMECs in our cytoadherence analysis. Given the decreased levels of SBP1 observed in the Maurer's clefts of infected erythrocytes, this reduction was likely due to ER stress (Fig. 3c, d), which as previously reported, may impair protein vesicular trafficking in malaria parasites[55,56]. Notably, DGAT1 deficiency has been shown to cause aberrant protein trafficking in human enterocytes[57], although the underlying mechanism remains still unclear and warrants further investigation. One possible explanation for these observations is that alterations in the balance between TAG and DAG, as well as in the phospholipid composition, under ER stress may contribute to defective protein trafficking. This is plausible because membrane compositions, particularly the levels of PE, PS, and DAG, are known to influence membrane and vesicle fusion processes[9]. In addition, the mislocalization of PfEMP1 may also hinder

cytoadherence by disrupting the cellular membrane architecture required for PfEMP1 assembly, possibly due to the excess generation of phospholipids resulting an abnormal phospholipid supply to the membrane (Fig. S1, S2). It is important to note that the cytoadherence assay, including analyses of ER stress and NL quantification, was performed at 96 hpi, a time point when some parasites were already dead, exhibiting morphological abnormalities. To specifically assess the intrinsic effect of PfDGAT deficiency, we selectively counted visually viable parasites with normal morphology under the microscope; however, we cannot rule out the possibility that some dead parasites partially influenced these assay results.

Recently, LDs, generated primarily by DGAT1, have been shown to participate in multiple aspects of cellular metabolism, including the formation of MCSs with other organelles to exchange fatty acids and glycerophospholipids[58-60]. It has been observed that LDs in *P. falciparum* form MCSs with nuclei, digestive vacuoles, the ER, mitochondria, and cytostomes, although their precise functions and associated proteins remain unresolved[46]. Therefore, further investigations of PfDGAT may help reveal unknown aspects of malaria parasite biology.

Methods

Ethics statement

The experiments with human erythrocytes were approved by the ethics committee of Nagasaki University (Approved#: 191226226). Human erythrocytes were purchased from the Japan Red Cross Society (Tokyo, Japan) (No: R030027). Informed consent was obtained by the Japan Red Cross Society before the blood samples were purchased (donor information was not disclosed to the purchaser). All ethical regulations relevant to human research participants were followed.

Parasite culture

Plasmodium falciparum NF54::DiCre strain (kindly gifted from Moritz Treeck) was cultured in O^+ erythrocytes at 5% hematocrit in RPMI-1640 medium (Gibco, Thermo Fisher Scientific, Waltham, MA, USA) supplemented with 5.95 mg/mL HEPES, 0.05 mg/mL hypoxanthine (Sigma-Aldrich, Merck, Darmstadt, Germany), 2 mg/mL sodium bicarbonate (Fujifilm Wako Chemical Corporation, Osaka, Japan), 10 µg/mL gentamicin (Gibco), and 0.5% Albumax II (Gibco) (RPMI-1640 complete media) and maintained at 37 °C in a gas mixture of 5% O_2, 5% CO_2, and 90% N_2, as previously described[4].

Generation of *Pfdgat*:LoxPint:HA line

To conditionally knock out *Pfldgat*, we generated a pSLI-*Pfdgat*-LoxP-3×2A-HA plasmid to introduce LoxP sites into *Pfldgat* utilizing an SLI method[31]. To create pSLI-*Pfdgat*-LoxP-3×2A-HA, pSLI-*Pflplat1*-LoxP-3×2A-HA[61] was linearized at the *Bgl*II and *Xma*I restriction sites. Synthetic DNA containing a LoxP site followed by 3′ recodonized *Pfdagt*, triple influenza hemagglutinin (HA) sequences, a 2A self-cleaving peptide sequence, a neomycin resistance gene cassette, a LoxP site, and a GFP reporter gene was obtained (Azenta Life Sciences, Burlington, MA, USA). The 5' genomic *Pfdgat* was amplified from the genomic DNA of NF54::DiCre strain with CloneAmp HiFi PCR Premix (Takara Bio, Shiga, Japan) using the primers listed in Table S1. These sequences were introduced into linearized pSLI-*Pflplat1*-LoxP-3x2A-HA using an In-Fusion HD Cloning Kit (Takara Bio).

For plasmid DNA transfection, trophozoite and schizont-stage parasites were collected using MACS magnetic columns (Miltenyi Biotec, Bergisch Gladbach, Germany). Plasmids were electroporated into erythrocytes using a GenePulser Xcell (Bio-Rad, Hercules, CA, USA) with cuvettes (Bio-Rad). Collected parasites were incubated with electroporated erythrocytes in RPMI-1640 complete medium for 48 hours. After 48 hours, parasites were selected with 1 nM WR99210 (Sigma-Aldrich) for 3–4 weeks followed by 400 µg/mL G418 (Fujifilm Wako Pure Chemical Corporation) for 2 weeks. Clonal parasites were obtained by limiting dilution of drug-selected transgenic parasites. To confirm plasmid integration into the

genome of clonal parasites, genomic DNA was extracted using a DNeasy Blood & Tissue Kit (QIAGEN, Hilden, Germany) and a diagnostic PCR was performed using the primers listed in Table S1.

Three-dimensional construction of PfDGAT and HsDGAT1

For the structural overlay of PfDGAT and HsDGAT1, Protein Data Bank files were retrieved from the AlphaFold Protein Structure Database (https://alphafold.ebi.ac.uk/) (PfDGAT; AF-O97295-F1-model_v4, HsDGAT1; AF-O75907-F1-model_v4). The proteins were visualized and superimposed using PyMOL (v3.1.4.1) (Schrödinger, USA).

Multiple sequence alignment of DGAT1

For multiple alignment of DGAT1 sequences, amino acid sequences were obtained from the NCBI database (https://www.ncbi.nlm.nih.gov/) (*Homo sapiens* DGAT1 [HsDGAT1], NP_036211.2; *Plasmodium falciparum* 3D7 DGAT [PfDGAT], XP_001351293; *Plasmodium vivax* P01 DGAT [PvDGAT], XP_001614490; *Plasmodium knowlesi* strain H DGAT [PkDGAT], XP_002258826; *Plasmodium berghei* ANKA DGAT [PbDGAT], XP_678753; *Toxoplasma gondii* ME49 DGAT [TgDGAT], XP_018638224; *Cryptosporidium parvum* IowaII DGAT [CpDGAT], XP_625364). The alignment was carried out using CLUSTALW

(v2.1). Sequence logos were created using WebLogo (v2.8.2) (https://weblogo.berkeley.edu/logo.cgi).

Growth assay

For growth assays, parasites were synchronized with 5% D-sorbitol (Fujifilm Wako Pure Chemical Corporation) and seeded into 24-well plates. Synchronized parasites were maintained in 1 mL of RPMI-1640 complete medium at 5% hematocrit and treated with either 100 nM rapamycin (Sigma-Aldrich) or an equivalent volume of dimethyl sulfoxide. Parasitemia was monitored daily using a Sysmex XN-30 hematology analyzer (Sysmex Corporation, Hyogo, Japan)[62] and maintained below 5% by serial passaging. For analysis, membranes of parasitized erythrocytes were permeabilized with CELLPACK DCL (Sysmex Corporation), and parasite nucleic acids were stained with Fluorocell M and Lysercell M (Sysmex Corporation). Growth curves were generated using GraphPad Prism v10.5.0 (GraphPad Software, San Diego, CA, USA).

Quantification of parasite stage distribution

For the quantification of parasite stage distribution, trophozoite- and schizont-stage parasites were collected using MACS magnetic columns (Miltenyi Biotec). Pelleted samples were resuspended at 2% hematocrit in RPMI-1640 complete medium for 4 hours under

continuous agitation at 40 rpm to reduce multiple infections of parasites within a single erythrocyte. After 4 hours of incubation, parasites were tightly synchronized with 5% D-sorbitol (0–4 hours post invasion) and seeded into 6-well plates. Thin blood smears were prepared at each time point and stained with Giemsa's azur eosin methylene blue solution (Sigma-Aldrich). Parasite staging was performed manually under light microscopy.

Immunofluorescence assay

Infected erythrocytes were immobilized on poly-D-lysine–coated coverslips (Thorlabs, NJ, USA; poly-D-lysine from MP Biomedicals, CA, USA). After immobilization, samples were fixed with 4% paraformaldehyde (Electron Microscopy Sciences, PA, USA) in phosphate-buffered saline (PBS) for 10 minutes, followed by crosslinking with 50 mM dimethyl suberimidate dihydrochloride (Sigma-Aldrich) in borate buffer for 20 minutes, and quenched with 10 mM glycine in PBS for 30 minutes. Fixed samples were permeabilized with 0.3% Triton X-100 (Fujifilm Wako Pure Chemical Corporation) in PBS and blocked with 1% skim milk in 0.05% Tween 20 (Tokyo Chemical Industry, Tokyo, Japan) in PBS for 60 minutes. Samples were incubated with primary antibodies overnight and with secondary antibodies for 60 minutes, followed by mounting in VECTASHIELD Antifade Mounting Medium with DAPI (Vector Laboratories, CA, USA). Immunostained samples were observed

using a 100× objective on an LSM780 confocal laser scanning microscope (Carl Zeiss, Oberkochen, Germany).

Western blot

For western blot analysis, parasites were collected using MACS magnetic columns (Miltenyi Biotec) and lysed in 0.03% saponin solution for 5 minutes. Collected samples were dissolved in lysis buffer (4% SDS, 0.5% Triton X-100, 25–75 U DNase I [Takara Bio] and cOmplete protease inhibitor cocktail [Roche, Basel, Switzerland] in 0.5% PBS) and denatured with SDS sample buffer containing dithiothreitol. Lysates were boiled at 50 °C for 3 minutes (PfDGAT-HA) or at 95 °C for 10 minutes (Phospho-PfeIF2α), separated on 4%–12% polyacrylamide gels (Invitrogen), and transferred to PVDF membranes. Membranes were blocked with Bullet Blocking One (Nacalai Tesque, Kyoto, Japan), incubated overnight with primary antibodies, then incubated for 30 minutes with horseradish peroxidase (HRP)-conjugated secondary antibodies. Signals were detected using chemiluminescent HRP substrate (Thermo Fisher Scientific) and visualized with WSE-6100 LuminoGraph I (ATTO, Tokyo, Japan).

For internal control detection of PfAldolase, membranes were stripped with WB Stripping Solution Strong (Nacalai Tesque) for 30 minutes, re-blocked with Bullet Blocking One,

incubated with HRP-conjugated anti-*Plasmodium* aldolase antibody for 30 minutes, and the signal was developed with chemiluminescent HRP substrate (Thermo Fisher Scientific) for 5 minutes.

Gametocytogenesis

Gametocyte production was induced by initiating cultures at 6% hematocrit in complete RPMI medium supplemented with 10% human serum (Japan Red Cross, lot #28J0058) and 0.1% parasitemia[4] (day 1). Hematocrit was reduced to 3% on day 4. Asexual parasites were eliminated by treatment with 50 mM N-acetyl glucosamine (Sigma-Aldrich) to remove asexual parasites on days 9–11 and treated with 100 nM rapamycin (Sigma-Aldrich) from day 10 onward to induce conditional knockout. Gametocytemia and parasite stage distribution were assessed manually from Giemsa-stained blood smears on days 12–15. Media were replaced with pre-warmed and fresh media every day up to day 15. To investigate the gametocyte conversion rate, parasites were synchronized with 5% D-sorbitol and incubated with 100 nM rapamycin for 24 hours. After treatment, trophozoite- and schizont-stage parasites were collected using MACS magnetic columns (Miltenyi Biotec) and maintained with 10–15 times the volume of erythrocytes to parasite for 24 hours (day 0). The parasites were treated with 50 mM NAG (Sigma-Aldrich) on days 1–4. Giemsa-stained blood films were created to count ring-stage parasitemia on day 1 and gametocytemia on

days 5–8. The gametocyte conversion rate was calculated by dividing the gametocytemia count on day 5 by the parasitemia count on day 1. For the extraction of genomic DNA from gametocytes, parasites were enriched at the interface between 40% and 60% Percoll layers and subsequently collected using MACS magnetic columns (Miltenyi Biotec). Genomic DNA was extracted using a DNeasy Blood & Tissue Kit (Qiagen), and PCR was performed using the primers listed in Table S1.

Quantitative reverse transcription PCR

For quantitative reverse transcription PCR (qRT-PCR), infected erythrocytes were suspended in 10 volumes of TRIzol (Invitrogen, Thermo Fisher Scientific, Waltham, MA, USA) relative to erythrocyte volume and stored at −80°C until use. From the suspension, RNA was extracted with a PureLink RNA Mini Kit (Invitrogen), and cDNA was synthesized from 0.1–1 µg of the RNA using a ReverTra Ace qPCR RT kit (Toyobo, Osaka, Japan). Specific DNA regions of AP2-G and the housekeeping gene seryl-tRNA synthetase (PF3D7_0717700) were amplified from the cDNA using a KAPA SYBR Fast qPCR kit (Kapa Biosystems, MA, USA) and a QuantStudio 3 Real-Time PCR System (Applied Biosystems, Thermo Fisher Scientific, Waltham, MA, USA) with the primers listed in Table S1[63]. Relative quantification of the gene expression was performed using the comparative CT method.

Neutral lipid quantification

For neutral lipid (NL) quantification, parasites were synchronized at 0–4 hpi and maintained in the presence or absence of 100 nM rapamycin until 96, 144, and 192 hpi. NLs were stained with HCS LipidTOX Red (Invitrogen; 1:1000 dilution) for 30 minutes at 37 °C, washed with RPMI-1640 without Phenol Red (Nacalai Tesque), and counterstained with Hoechst 33342 nuclear stain (Sigma-Aldrich) for 5 minutes. Stained samples were observed under a Leica DMi8 inverted microscope (Leica Microsystems, Wetzlar, Germany). Fluorescence signal intensity was analyzed using ImageJ software (National Institutes of Health, MD, USA).

SBP1 quantification

For SBP1 quantification, the parasite was synchronized with 5% D-sorbitol and maintained in the presence or absence of 100 nM rapamycin. Six and 8 days after the treatments, the infected erythrocytes were immunostained with rabbit anti-SBP1 antibody[42], followed by Alexa Fluor 594-conjugated goat anti-rabbit antibody. The immunofluorescence signal for SBP1 was visualized using an LSM780 confocal laser scanning microscope (Carl Zeiss) equipped with a Plan-Apochromat 100×/1.40 Oil DIC M27 (numerical aperture = 1.40). The scanned micrographs were processed using ImageJ software (National Institutes of Health). The SBP1 signal was defined using the Mean method on Threshold menu, and

subsequently quantified using the Analyze Particles function after applying Dilate to enhance signal continuity and the Watershed algorithm to separate continuous particles.

Cytoadherence assay

For the static cytoadherence assay, immortalized human brain microvascular endothelial cells (HBMEC) (P10361-IM; Innoprot, Dario, Spain) were cultivated on 13-mm coverslips (Matsunami Glass, Osaka, Japan) in 24-well plates containing Endothelial Cell Medium (P60104; Innoprot, hereafter referred to as HBMEC medium) supplemented with 5% fetal bovine serum (175012; Nichirei Biosciences, Tokyo, Japan). They were maintained at 37 °C in a humidified 5% CO_2 atmosphere and used at 80%–90% confluence on day 7. HBMEC-panned parasites, obtained as previously reported[64,65], were maintained at 4% hematocrit with or without 100 nM rapamycin on day 6, followed by their synchronization with D-sorbitol. On day 7, HBMEC-panned parasites were adjusted to 1%–2% parasitemia at 4% hematocrit across groups. Parasite suspension (200 µL per well) was seeded onto HBMEC monolayers in RPMI-1640 complete medium and incubated at 37 °C for 75 minutes. During incubation, the plate was gently agitated every 30 minutes to resuspend the settled red blood cells. After 75 minutes, the medium was removed from each well, and HBMECs were gently washed with RPMI medium. This washing step was repeated five times in total. After the second or third wash, the coverslips were transferred to a new 24-well plate, and

the remaining washes were performed. After removing the medium, 2.5% glutaraldehyde (400 μL per well, Sigma-Aldrich) in 1% PBS was added to each well and incubated overnight for fixation. The fixative was then removed, and the samples were stained with Giemsa's azur eosin methylene blue solution (Sigma-Aldrich) for 15 minutes. The coverslips were covered and air-dried for about 2 days. Finally, they were mounted onto glass slides with the cell-adherent side facing down and secured for microscopic observation.

For the flow cytoadherence assay, HBMECs were seeded onto μ-Slide VI 0.1 microfluidic channel slides (80666; Ibidi, Gräfelfing, Germany). They were maintained at 37 °C in a humidified 5% CO_2 atmosphere and used at 80%–90% confluence on day 7. On day 7, synchronized HBMEC-panned parasites were adjusted to 1%–2% parasitemia at 2% hematocrit across groups. After replacing the HBMEC medium in the channel slides, the parasites were maintained at 38 °C on a hot plate. The parasite suspension was then continuously perfused through the slides at a shear stress of 6 dyn/cm² (flow rate: 6.33 mL/min) for 20 minutes per lane using a peristaltic pump (AC-2110II-3; ATTO), followed by flushing with RPMI-1640 medium for an additional 20 minutes per lane. The suspension was introduced through one inlet connected to silicone tubing (3 mm diameter), while RPMI-1640 medium was simultaneously perfused through the other. After parasite perfusion was completed in each lane, the channel was immediately washed with RPMI-1640 medium.

Prior to the introduction of a new sample, RPMI-1640 was perfused through the tubing to wash it. After all lanes had been washed, 2.5% glutaraldehyde in 1% PBS was gently perfused through the slides to achieve fixation, and 20–30 images were acquired per lane.

Liquid chromatography-mass spectrometry analysis

For liquid chromatography-mass spectrometry analysis, parasites were purified at 78 hpi with a magnetic column, and total lipids were extracted with 50 volumes of 2-propanol relative to the volume of parasite pellets. The extracted lipids were analyzed for phospholipids using a triple quadrupole mass spectrometer coupled to a Nexera liquid chromatography system (LCMS-8050 system, Shimadzu) according to a previously published protocol[66]. Briefly, the extracted lipids were separated on an Acquity UPLC BEH C8 column (1.7 µm, 2.1 x 100 mm, Waters) with a gradient of mobile phase A (5 mM NH_4HCO_3 in water), mobile phase B (acetonitrile), and mobile phase C (2-propanol) at a flow rate of 0.35 ml/min. The gradient program (time (A:B:C%)) was as follows: 0 minutes (75:20:5), to 20 minutes (20:75:5), to 40 minutes (20:5:75), to 45 minutes (5:5:90), to 50 minutes (5:5:90), and to 55 minutes (75:20:5). The column oven temperature was set at 47 °C. The eluent was ionized by electrospray ionization, then analyzed in the mass spectrometer in selected reaction monitoring (SRM) mode. The SRM transitions (Q1 and Q3) for the head group of phospholipids were ([M + H]+, 184) for PC, ([M + H]+, neutral loss

of 141) for PE, ([M – H]–, neutral loss of 87) for PS, and ([M – H]–, 241) for PI. Peak identification and peak area integration were performed using LabSolutions software (Version 5.99 SP2, Shimadzu) according to the manufacturer's instructions. The peak area of each phospholipid species was divided by the sum of the total peak area for all detected phospholipids with the same head group and presented as the area ratio.

Triglyceride (TG) levels were measured using previously published LC-MS/MS method with minor modifications[67]. A triple quadrupole mass spectrometer (LCMS-8060; Shimadzu Co., Kyoto, Japan) coupled to a UHPLC system (Nexera; Shimadzu Co.) was used. The extracted lipids were separated on an Shim-pack Velox C18 column (2.1 × 50 mm, 2.7 μm; Shimadzu Co.) with a gradient of mobile phase A (20 mM NH_4HCO_2 in water), mobile phase B (acetonitrile), and mobile phase C (2-propanol) at a flow rate of 0.4 ml/min. The gradient program (time (A:B:C%)) was as follows: 0 minutes (15:15:70), to 0.1 minutes (15:15:70), to 8.4 minutes (5:20:75), to 9 minutes (5:20:75), to 9.1 minutes (15:15:70), and to 11 minutes (15:15:70). The column oven temperature was set at 45°C. The eluent was ionized by electrospray ionization and analyzed in selected reaction monitoring (SRM) mode. For each SRM transition, Q1 was set to the ammonium-adduct parent ion and Q3 to the neutral loss corresponding to a fatty acyl chain. Instrument operation was controlled using Shimadzu LabSolutions LCMS software, version 5.112 (Shimadzu Co.). Species-level TG annotations

were expressed as the total number of carbon atoms and the total number of double bonds of the three fatty acyl chains. Observed TG peaks were named as the species-level TG annotation followed by the fatty acyl chain detected as the neutral loss. TG peaks that exhibited a peak height of ≥100,000 in all samples within any group were selected for quantification. Peak areas for peaks with a peak height of ≥30,000 were calculated using Traces software[66].

Statistics and data reproducibility

Data normality was checked using the Shapiro–Wilk test. Statistical significance is shown in each graph via a P value. A P value of less than 0.05 was considered statistically significant. Statistical tests were performed using GraphPad Prism (v10.5.0).

Data availability

All source data and uncropped gel and blotting images are included in a Source Data file.

Acknowledgments

This work was partially supported by Grants-in-Aid for Scientific Research (KAKENHI), grant numbers 17K08805 (F.T.), 23K06518 (F.T.), 21K15429 (J.F.), and 25K18790 (J.F.); the Japan Institute for Health Security (JIHS) Intramural Research Fund (22T001 to HS); and by a foundation from Shionogi and Co., Ltd. These funders were not involved in the design, experiments, or data analyses in this study. We thank Suzanne Leech, Ph.D., from Edanz (https://jp.edanz.com/ac) for editing a draft of this manuscript.

Author contributions

Conceptualization: M.Y., J.F., S.M., S.M.T., H.O., and F.T. Data collection: J.F., M.Y., S.M., M.T., S.M.T., and H.O. Data analysis: J.F., M.Y., S.M., M.T., S.M.T., H.O., and F.T. Funding acquisition: J.F., and F.T. Supervision: J.F., and F.T. Writing – original draft: M.Y., J.F., and F.T. Writing – review & editing: M.Y., J.F., S.M., S.M.T., M.T., H.O., T.S., Y.O., K.Y., E.T., D.K.I., K.K., and F.T. Resources: F.T., K.Y., and K.K.

Competing interests

No competing interests are declared.

Figure legends

Fig. 1. PfDGAT contains conserved DAGT1 functional motifs and the characteristic MBOAT motif

(a) Superimposed three-dimensional structures of PfDGAT and HsDGAT1. Structural data were obtained from the AlphaFold Protein Structure Database. The FYXDWWN and SXXXHEY motifs are shown as the sticks, and the other regions as the cartoon; the motifs are magnified in the right insets. (b) Multiple sequence alignment of DGAT1 orthologs from humans and apicomplexan parasites. Amino acid residues shared in ≥ 50% of the analyzed organisms are highlighted in yellow. The FYXDWWN and SXXXHEY motifs, as well as the MBOAT motif B, are enclosed in black rectangles. Acidic, basic, polar, nonpolar, aromatic, and sulfur-containing amino acids are shown as magenta, red, green, blue, orange, and purple letters, respectively, in the upper sequence logo.

Fig. 2. Establishment of PfDGAT conditional knockout *P. falciparum* lines

(a) Putative phospholipid metabolic pathways in *P. falciparum.* PfLPLAT1, *P. falciparum* lysophospholipid acyltransferase 1; the first LPLAT identified in this parasite, functions in both the Kennedy pathway and the Lands' cycle[61]. G3P, glyceraldehyde 3-phosphate; LPA, lysophosphatidic acid; PA, phosphatidic acid; CDP-DAG, cytidine diphosphate diacylglycerol; PG, phosphatidylglycerol; PI, phosphatidylinositol; PS, phosphatidylserine;

PE, phosphatidylethanolamine; PC, phosphatidylcholine; LPG, lysophosphatidylglycerol; LPI, lysophosphatidylinositol; LPS, lysophosphatidylserine; LPE, lysophosphatidylethanolamine; LPC, lysophosphatidylcholine; PfGPAT1 and PfGPAT2, *P. falciparum* glycerol-3-phosphate acyltransferase 1 and 2; PfLPLAT1, *P. falciparum* lysophosphatidic acid acyltransferase 1; and PLA2, phospholipase A2. (b) Design of *Pfdgat* conditional gene knockout with the DiCre system. The 5' homologous region of *Pfdgat* contains 654 base pairs, beginning from the start codon. Upon rapamycin treatment, the recodonized region, flanked by LoxP introns and containing the FYXDWWN and SXXXHEY motifs, was excised from the parasite genome. Arrows indicate the transcription initiation site and the primer binding sites for PCR-based tests. (c) Diagnostic PCR showed that the target gene was successfully replaced with the targeting constructs: DNA segments were correctly amplified with f1/r1 (NF54::DiCre, not amplified; *Pfdagt*:LoxPint:HA B10 and G12 clones, 3704 bp), f2/r2 (NF54::DiCre, not amplified; *Pfdagt*:LoxPint:HA B10 and G12, 756 bp), and f1/r2 (NF54::DiCre, 1077 bp; *Pfdagt*:LoxPint:HA B10 and G12, not amplified) primer sets. (d, e) Conditional gene knockout of *Pfdagt* was confirmed by PCR and western blotting. (d) The size of DNA amplicons for the 5’ segment shifted from 3704 bp to 1089 bp in *Pfdagt*:LoxPint:HA B10 and G12 after 24 hours of rapamycin treatment. (e) Decreased expression of PfDAGT was detected in *Pfdagt*:LoxPint:HA B10 and G12 with anti-HA antibody after 24 hours of rapamycin treatment. PfAldolase was used as an internal protein

control. Theoretical molecular masses (kDa) of HA-tagged PfDAGT and PfAldolase are 81.6 and 40.0, respectively. Experiments were repeated three times with similar results. (f) Growth curve of +Rap or −Rap *Pfdagt*:LoxPint:HA B10 and G12. Data are shown as mean ± SD from n = 3 independent biological replicates. P values were calculated using two-way ANOVA followed by Tukey's HSD test. $^{*}P < 0.0001$ (−Rap vs. +Rap *Pfdagt*:LoxPint:HA B10); $^{\#}P < 0.0001$ (−Rap vs. +Rap *Pfdagt*:LoxPint:HA G12). Experiments were repeated twice with similar results. (g–i) Stage distributions of +Rap or −Rap *Pfdagt*:LoxPint:HA B10. (g) Representative images of Giemsa-stained blood films at described time points. (h, i) Bar charts showing the parasite stage distributions (h) and parasitemia of each stage (i) at the described time points (24, 48, 72, 96, 120, 144, 168, and 192 hours of post-infection [hpi]). Data are shown as mean ± SD from n = 3 independent biological replicates. (j) Representative confocal microscope images of *Pfdagt*:LoxPint:HA B10 co-stained for PfDAGT and ER-resident protein BiP. Samples were immunostained for PfDAGT using an anti-HA antibody (yellow) and for ER with an anti-BiP antibody (magenta). Scale bars = 2 μm. Source data are provided as a Source Data file.

Fig. 3. PfDGAT deficiency reduced NL levels and triggered ER stress in parasites

(a) Representative images of LipidTOX-stained +Rap or −Rap *Pfdagt*:LoxPint:HA at the described time points. Scale bars = 2 μm. (b) Boxplots showing the fluorescence intensity of

LipidTOX NL staining per area in +Rap or −Rap *Pfdagt*:LoxPint:HA at 96, 144, and 196 hpi. Vertical lines range from the minimum to the maximum values. Horizontal lines represent the 25th percentile (bottom), median (middle), and 75th percentile (top). P values were calculated using Mann–Whitney U test. Experiments were repeated twice. (c) Western blot analysis of phospho-PfeIF2α (P-PfeIF2α) expression in +Rap and −Rap *Pfdagt*:LoxPint:HA after 216 hours of rapamycin treatment. PfAldolase was used as an internal control for the total amount of proteins. Theoretical molecular masses (kDa) of P-PfeIF2α and PfAldolase are 38.0 and 40.0, respectively. Experiments were repeated three times. (d) Bar charts showing the relative expression levels of P-PfeIF2α in +Rap and −Rap *Pfdagt*:LoxPint:HA after 216 hours of rapamycin treatment. Expression levels in the −Rap group were set to 1, and those in the +Rap group were normalized accordingly. P value was calculated using a paired, two-tailed *t*-test. Source data are provided as a Source Data file.

Fig. 4. PfDGAT deficiency led to altered TAG profiles in the parasites.

(a–c) Bar graphs showing normalized fractions of triacylglycerol (TAG) species against the total area values of TAGs in +Rap and −Rap *Pfdagt*:LoxPint:HA at 78 hpi. On the x-axis, TAGs are denoted as TG. The numbers following an "TG" indicate the total number of carbon atoms and double bounds (e.g., TG 46:0), and the values following “FA” specify the identified acyl chain among the three (e.g., FA 16:0). Data are shown as mean + SD from n

= 3 independent biological replicates. P values were calculated using unpaired two-tailed t-test (*P < 0.05, **P < 0.01, ***P < 0.005, ****P < 0.001). Source data are provided as a Source Data file.

Fig. 5. PfDGAT deficiency abolished gametocytogenesis without any effects on gametocyte development

(a) Schematics of experimental procedure to investigate the effect of PfDGAT deficiency on gametocyte development in *Pfdagt*:LoxPint:HA. (b) Conditional knockout of *Pfdagt* in gametocytes was confirmed by PCR on day 14. The size of DNA amplicons shifted from 3704 bp to 1089 bp. (c) Gametocytemia of +Rap or −Rap *Pfdagt*:LoxPint:HA on days 12–15. Data are shown as mean ± SD from n = 3 independent biological replicates. (d) Bar charts showing the gametocyte stage distributions of +Rap or −Rap *Pfdagt*:LoxPint:HA on days 12–15. Data are shown as mean from n = 3 independent biological replicates. (e) Schematics of experimental procedure to investigate the effect of PfDGAT deficiency on sexual conversion rate in *Pfdagt*:LoxPint:HA. (f) Conditional knockout of *Pfdagt* in trophozoites and schizonts was confirmed by PCR on day 0. The size of DNA amplicons shifted from 3704 bp to 1089 bp. (g) Comparison of sexual conversion rates between +Rap and −Rap *Pfdagt*:LoxPint:HA parasites on day 5. P values were calculated using Mann–Whitney U test. Data are shown as mean ± SD from n = 4 independent biological

replicates. Experiments were repeated three times with similar results. (h) Comparison of gametocytemia in +Rap and −Rap *Pfdagt*:LoxPint:HA parasites on days 5–9. P values were calculated using two-way ANOVA followed by Šídák's multiple comparison test. *$P < 0.0001$ (−Rap vs. +Rap *Pfdagt*:LoxPint:HA). Data are shown as mean ± SD from n = 4 independent biological replicates. Experiments were repeated three times with similar results. Fig. 5a and e were created with Biorender.com. Source data are provided as a Source Data file.

Fig. 6. PfDGAT deficiency impaired cytoadhesion of parasites on human brain endothelial cells

(a) Schematics of cytoadhesion assay under static and flow conditions. (b, c) Dot plots showing the number of erythrocytes infected with *Pfdgat*:LoxPint:HA parasites that adhered to 100 human brain microvascular endothelial cells (HBMECs) under static (b) and flow (c) conditions after 6 days of rapamycin treatment. Data are shown as mean ± SD from n = 3 independent biological replicates (b) and from n = 2 independent biological replicates from 3 independent experiments (c). P values were calculated using one-way ANOVA followed by Tukey–Kramer test. BFA, brefeldin. (d) Dot plots showing the number of SBP1 puncta on infected erythrocytes with *Pfdagt*:LoxPint:HA on 6 and 8 days of rapamycin treatment. P values were calculated using one-way ANOVA followed by Tukey–Kramer test. Representative immunofluorescence images are shown above the corresponding plots.

Samples were stained for SBP1 with rabbit anti-SBP1 antibody (red) and for nuclei with DAPI (blue). Scale bars = 2 μm. Fig. 6a was created with Biorender.com. Source data are provided as a Source Data file.

Fig. 7. Schematic diagram illustrating the proposed effects of *Pfdgat* deletion on parasites

(1) Deletion of PfDGAT results in elevated free fatty acid (FFA) levels and/or acyl-CoAs due to the decreased incorporation of acyl-CoAs into diacylglycerols (DAGs). (2) Elevated acyl-CoA levels lead to increased phospholipid synthesis. (3) The parasite senses high phospholipid levels as a favorable environment for its asexual replication and therefore suppresses gametocyte differentiation. (4, 5) An excess of FFAs, possibly resulting from increased unused acyl-CoAs, triggers ER stress. A reduction in LDs further exacerbates this stress and ultimately leads to parasite death. (6) ER stress and alterations in membrane lipid composition adversely affect vesicular protein trafficking. (7) Impaired vesicular trafficking reduces the surface presentation of cytoadhesive molecules, such as PfEMP1, thereby diminishing the capacity of parasites to adhere to human endothelial microvascular cells. Created with BioRender.com.

References

1 Vielemeyer, O., McIntosh, M. T., Joiner, K. A. & Coppens, I. Neutral lipid synthesis and storage in the intraerythrocytic stages of Plasmodium falciparum. *Mol Biochem Parasitol* **135**, 197-209 (2004). https://doi.org/10.1016/j.molbiopara.2003.08.017

2 Mitamura, T., Hanada, K., Ko-Mitamura, E. P., Nishijima, M. & Horii, T. Serum factors governing intraerythrocytic development and cell cycle progression of Plasmodium falciparum. *Parasitol Int* **49**, 219-229 (2000). https://doi.org/10.1016/s1383-5769(00)00048-9

3 Hsiao, L. L., Howard, R. J., Aikawa, M. & Taraschi, T. F. Modification of host cell membrane lipid composition by the intra-erythrocytic human malaria parasite Plasmodium falciparum. *Biochem J* **274** (Pt 1), 121-132 (1991). https://doi.org/10.1042/bj2740121

4 Tanaka, T. Q. *et al.* Polyunsaturated fatty acids promote Plasmodium falciparum gametocytogenesis. *Biol Open* **8** (2019). https://doi.org/10.1242/bio.042259

5 Tran, P. N. *et al.* Changes in lipid composition during sexual development of the malaria parasite Plasmodium falciparum. *Malar J* **15**, 73 (2016). https://doi.org/10.1186/s12936-016-1130-z

792 6 Gulati, S. *et al.* Profiling the Essential Nature of Lipid Metabolism in Asexual Blood
793 and Gametocyte Stages of Plasmodium falciparum. *Cell Host Microbe* **18**, 371-381
794 (2015). https://doi.org/10.1016/j.chom.2015.08.003
795 7 Chernomordik, L. V., Zimmerberg, J. & Kozlov, M. M. Membranes of the world unite! *J*
796 *Cell Biol* **175**, 201-207 (2006). https://doi.org/10.1083/jcb.200607083
797 8 Joardar, A., Pattnaik, G. P. & Chakraborty, H. Mechanism of Membrane Fusion:
798 Interplay of Lipid and Peptide. *J Membr Biol* **255**, 211-224 (2022).
799 https://doi.org/10.1007/s00232-022-00233-1
800 9 Torng, T. & Wickner, W. Phosphatidylinositol and phosphatidylinositol-3-phosphate
801 activate HOPS to catalyze SNARE assembly, allowing small headgroup lipids to
802 support the terminal steps of membrane fusion. *Mol Biol Cell* **32**, ar19 (2021).
803 https://doi.org/10.1091/mbc.E21-07-0373
804 10 Callan-Jones, A., Sorre, B. & Bassereau, P. Curvature-driven lipid sorting in
805 biomembranes. *Cold Spring Harb Perspect Biol* **3** (2011).
806 https://doi.org/10.1101/cshperspect.a004648
807 11 Choudhary, V., Ojha, N., Golden, A. & Prinz, W. A. A conserved family of proteins
808 facilitates nascent lipid droplet budding from the ER. *J Cell Biol* **211**, 261-271 (2015).
809 https://doi.org/10.1083/jcb.201505067

810 12 Fujimoto, T., Ohsaki, Y., Cheng, J., Suzuki, M. & Shinohara, Y. Lipid droplets: a
811 classic organelle with new outfits. *Histochem Cell Biol* **130**, 263-279 (2008).
812 https://doi.org/10.1007/s00418-008-0449-0
813 13 Olzmann, J. A. & Carvalho, P. Dynamics and functions of lipid droplets. *Nat Rev Mol*
814 *Cell Biol* **20**, 137-155 (2019). https://doi.org/10.1038/s41580-018-0085-z
815 14 Pressly, J. D. *et al.* Adaptive and maladaptive roles of lipid droplets in health and
816 disease. *Am J Physiol Cell Physiol* **322**, C468-C481 (2022).
817 https://doi.org/10.1152/ajpcell.00239.2021
818 15 Chen, G., Harwood, J. L., Lemieux, M. J., Stone, S. J. & Weselake, R. J.
819 Acyl-CoA:diacylglycerol acyltransferase: Properties, physiological roles, metabolic
820 engineering and intentional control. *Prog Lipid Res* **88**, 101181 (2022).
821 https://doi.org/10.1016/j.plipres.2022.101181
822 16 Kuerschner, L., Moessinger, C. & Thiele, C. Imaging of lipid biosynthesis: how a
823 neutral lipid enters lipid droplets. *Traffic* **9**, 338-352 (2008).
824 https://doi.org/10.1111/j.1600-0854.2007.00689.x
825 17 Yen, C. L., Monetti, M., Burri, B. J. & Farese, R. V., Jr. The triacylglycerol synthesis
826 enzyme DGAT1 also catalyzes the synthesis of diacylglycerols, waxes, and retinyl
827 esters. *J Lipid Res* **46**, 1502-1511 (2005).
828 https://doi.org/10.1194/jlr.M500036-JLR200

829 18 Stone, S. J. *et al.* Lipopenia and skin barrier abnormalities in DGAT2-deficient mice. *J*
830 *Biol Chem* **279**, 11767-11776 (2004). https://doi.org/10.1074/jbc.M311000200
831 19 Smith, S. J. *et al.* Obesity resistance and multiple mechanisms of triglyceride
832 synthesis in mice lacking Dgat. *Nat Genet* **25**, 87-90 (2000).
833 https://doi.org/10.1038/75651
834 20 Listenberger, L. L. *et al.* Triglyceride accumulation protects against fatty acid-induced
835 lipotoxicity. *Proc Natl Acad Sci U S A* **100**, 3077-3082 (2003).
836 https://doi.org/10.1073/pnas.0630588100
837 21 Palacpac, N. M. *et al.* Evidence that Plasmodium falciparum diacylglycerol
838 acyltransferase is essential for intraerythrocytic proliferation. *Biochem Biophys Res*
839 *Commun* **321**, 1062-1068 (2004). https://doi.org/10.1016/j.bbrc.2004.07.070
840 22 Zhang, M. *et al.* Uncovering the essential genes of the human malaria parasite
841 Plasmodium falciparum by saturation mutagenesis. *Science* **360** (2018).
842 https://doi.org/10.1126/science.aap7847
843 23 Palacpac, N. M. *et al.* Developmental-stage-specific triacylglycerol biosynthesis,
844 degradation and trafficking as lipid bodies in Plasmodium falciparum-infected
845 erythrocytes. *J Cell Sci* **117**, 1469-1480 (2004). https://doi.org/10.1242/jcs.00988

846 24 Guo, Z., Cromley, D., Billheimer, J. T. & Sturley, S. L. Identification of potential
847 substrate-binding sites in yeast and human acyl-CoA sterol acyltransferases by
848 mutagenesis of conserved sequences. *J Lipid Res* **42**, 1282-1291 (2001).
849 25 Wang, L. *et al.* Structure and mechanism of human diacylglycerol O-acyltransferase 1.
850 *Nature* **581**, 329-332 (2020). https://doi.org/10.1038/s41586-020-2280-2
851 26 Xu, J. *et al.* Cloning and characterization of an acyl-CoA-dependent diacylglycerol
852 acyltransferase 1 (DGAT1) gene from Tropaeolum majus, and a study of the
853 functional motifs of the DGAT protein using site-directed mutagenesis to modify
854 enzyme activity and oil content. *Plant Biotechnol J* **6**, 799-818 (2008).
855 https://doi.org/10.1111/j.1467-7652.2008.00358.x
856 27 Shindou, H., Eto, M., Morimoto, R. & Shimizu, T. Identification of membrane
857 O-acyltransferase family motifs. *Biochem Biophys Res Commun* **383**, 320-325 (2009).
858 https://doi.org/10.1016/j.bbrc.2009.04.013
859 28 Hofmann, K. A superfamily of membrane-bound O-acyltransferases with implications
860 for wnt signaling. *Trends Biochem Sci* **25**, 111-112 (2000).
861 https://doi.org/10.1016/s0968-0004(99)01539-x
862 29 Collins, C. R. *et al.* Robust inducible Cre recombinase activity in the human malaria
863 parasite Plasmodium falciparum enables efficient gene deletion within a single

864 asexual erythrocytic growth cycle. *Mol Microbiol* **88**, 687-701 (2013).
865 https://doi.org/10.1111/mmi.12206
866 30 Tiburcio, M. *et al.* A Novel Tool for the Generation of Conditional Knockouts To Study
867 Gene Function across the Plasmodium falciparum Life Cycle. *mBio* **10** (2019).
868 https://doi.org/10.1128/mBio.01170-19
869 31 Birnbaum, J. *et al.* A genetic system to study Plasmodium falciparum protein function.
870 *Nat Methods* **14**, 450-456 (2017). https://doi.org/10.1038/nmeth.4223
871 32 Nawabi, P., Lykidis, A., Ji, D. & Haldar, K. Neutral-lipid analysis reveals elevation of
872 acylglycerols and lack of cholesterol esters in Plasmodium falciparum-infected
873 erythrocytes. *Eukaryot Cell* **2**, 1128-1131 (2003).
874 https://doi.org/10.1128/EC.2.5.1128-1131.2003
875 33 Chitraju, C. *et al.* Triglyceride Synthesis by DGAT1 Protects Adipocytes from
876 Lipid-Induced ER Stress during Lipolysis. *Cell Metab* **26**, 407-418 e403 (2017).
877 https://doi.org/10.1016/j.cmet.2017.07.012
878 34 Zhang, M. *et al.* PK4, a eukaryotic initiation factor 2alpha(eIF2alpha) kinase, is
879 essential for the development of the erythrocytic cycle of Plasmodium. *Proc Natl Acad*
880 *Sci U S A* **109**, 3956-3961 (2012). https://doi.org/10.1073/pnas.1121567109

881 35 Zhang, M. *et al.* Inhibiting the Plasmodium eIF2alpha Kinase PK4 Prevents
882 Artemisinin-Induced Latency. *Cell Host Microbe* **22**, 766-776 e764 (2017).
883 https://doi.org/10.1016/j.chom.2017.11.005
884 36 Brancucci, N. M. B. *et al.* Lysophosphatidylcholine Regulates Sexual Stage
885 Differentiation in the Human Malaria Parasite Plasmodium falciparum. *Cell* **171**,
886 1532-1544 e1515 (2017). https://doi.org/10.1016/j.cell.2017.10.020
887 37 Sinha, A. *et al.* A cascade of DNA-binding proteins for sexual commitment and
888 development in Plasmodium. *Nature* **507**, 253-257 (2014).
889 https://doi.org/10.1038/nature12970
890 38 Kafsack, B. F. *et al.* A transcriptional switch underlies commitment to sexual
891 development in malaria parasites. *Nature* **507**, 248-252 (2014).
892 https://doi.org/10.1038/nature12920
893 39 Flick, K. & Chen, Q. var genes, PfEMP1 and the human host. *Mol Biochem Parasitol*
894 **134**, 3-9 (2004). https://doi.org/10.1016/j.molbiopara.2003.09.010
895 40 Crary, J. L. & Haldar, K. Brefeldin A inhibits protein secretion and parasite maturation
896 in the ring stage of Plasmodium falciparum. *Mol Biochem Parasitol* **53**, 185-192
897 (1992). https://doi.org/10.1016/0166-6851(92)90020-k

898 41 Wickham, M. E. *et al.* Trafficking and assembly of the cytoadherence complex in
899 Plasmodium falciparum-infected human erythrocytes. *EMBO J* **20**, 5636-5649 (2001).
900 https://doi.org/10.1093/emboj/20.20.5636
901 42 Omoda, A. *et al.* Skeleton binding protein 1 localizes to the Maurer's cleft and
902 interacts with PfHSP70-1 and PfHSP70-x in Plasmodium falciparum
903 gametocyte-infected erythrocytes. *Parasitol Int* **100**, 102864 (2024).
904 https://doi.org/10.1016/j.parint.2024.102864
905 43 Oppenheim, R. D. *et al.* BCKDH: the missing link in apicomplexan mitochondrial
906 metabolism is required for full virulence of Toxoplasma gondii and Plasmodium
907 berghei. *PLoS Pathog* **10**, e1004263 (2014).
908 https://doi.org/10.1371/journal.ppat.1004263
909 44 Olszewski, K. L. & Llinas, M. Central carbon metabolism of Plasmodium parasites.
910 *Mol Biochem Parasitol* **175**, 95-103 (2011).
911 https://doi.org/10.1016/j.molbiopara.2010.09.001
912 45 Cao, J. *et al.* Targeting Acyl-CoA:diacylglycerol acyltransferase 1 (DGAT1) with small
913 molecule inhibitors for the treatment of metabolic diseases. *J Biol Chem* **286**,
914 41838-41851 (2011). https://doi.org/10.1074/jbc.M111.245456

915 46 Lee, J., Matuschewski, K., van Dooren, G., Maier, A. G. & Rug, M. Lipid droplet
916 dynamics are essential for the development of the malaria parasite Plasmodium
917 falciparum. *J Cell Sci* **137** (2024). https://doi.org/10.1242/jcs.262162
918 47 Cui, W. *et al.* Free fatty acid induces endoplasmic reticulum stress and apoptosis of
919 beta-cells by Ca2+/calpain-2 pathways. *PLoS One* **8**, e59921 (2013).
920 https://doi.org/10.1371/journal.pone.0059921
921 48 Cho, H. *et al.* Signaling dynamics of palmitate-induced ER stress responses mediated
922 by ATF4 in HepG2 cells. *BMC Syst Biol* **7**, 9 (2013).
923 https://doi.org/10.1186/1752-0509-7-9
924 49 Wang, D., Wei, Y. & Pagliassotti, M. J. Saturated fatty acids promote endoplasmic
925 reticulum stress and liver injury in rats with hepatic steatosis. *Endocrinology* **147**,
926 943-951 (2006). https://doi.org/10.1210/en.2005-0570
927 50 Volmer, R., van der Ploeg, K. & Ron, D. Membrane lipid saturation activates
928 endoplasmic reticulum unfolded protein response transducers through their
929 transmembrane domains. *Proc Natl Acad Sci U S A* **110**, 4628-4633 (2013).
930 https://doi.org/10.1073/pnas.1217611110
931 51 Velazquez, A. P., Tatsuta, T., Ghillebert, R., Drescher, I. & Graef, M. Lipid
932 droplet-mediated ER homeostasis regulates autophagy and cell survival during
933 starvation. *J Cell Biol* **212**, 621-631 (2016). https://doi.org/10.1083/jcb.201508102

934 52 Schuck, S., Prinz, W. A., Thorn, K. S., Voss, C. & Walter, P. Membrane expansion
935 alleviates endoplasmic reticulum stress independently of the unfolded protein
936 response. *J Cell Biol* 187, 525-536 (2009). https://doi.org/10.1083/jcb.200907074
937 53 Soltysik, K., Ohsaki, Y., Tatematsu, T., Cheng, J. & Fujimoto, T. Nuclear lipid droplets
938 derive from a lipoprotein precursor and regulate phosphatidylcholine synthesis. *Nat*
939 *Commun* 10, 473 (2019). https://doi.org/10.1038/s41467-019-08411-x
940 54 Unal, S., Kina, U. Y., Kamil, M., Aly, A. S. I. & Palabiyik, B. Drug-induced ER stress
941 leads to induction of programmed cell death pathways of the malaria parasite.
942 *Parasitol Res* 123, 263 (2024). https://doi.org/10.1007/s00436-024-08281-3
943 55 Amodio, G. *et al.* Endoplasmic reticulum stress reduces COPII vesicle formation and
944 modifies Sec23a cycling at ERESs. *FEBS Lett* 587, 3261-3266 (2013).
945 https://doi.org/10.1016/j.febslet.2013.08.021
946 56 Ota, T., Gayet, C. & Ginsberg, H. N. Inhibition of apolipoprotein B100 secretion by
947 lipid-induced hepatic endoplasmic reticulum stress in rodents. *J Clin Invest* 118,
948 316-332 (2008). https://doi.org/10.1172/JCI32752
949 57 Schlegel, C. *et al.* Reversible deficits in apical transporter trafficking associated with
950 deficiency in diacylglycerol acyltransferase. *Traffic* 19, 879-892 (2018).
951 https://doi.org/10.1111/tra.12608

952 58 Miner, G. E. *et al.* PLIN5 interacts with FATP4 at membrane contact sites to promote
953 lipid droplet-to-mitochondria fatty acid transport. *Dev Cell* **58**, 1250-1265 e1256
954 (2023). https://doi.org/10.1016/j.devcel.2023.05.006
955 59 Hong, Z. *et al.* Mitoguardin-2-mediated lipid transfer preserves mitochondrial
956 morphology and lipid droplet formation. *J Cell Biol* **221** (2022).
957 https://doi.org/10.1083/jcb.202207022
958 60 Chang, C. L. *et al.* Spastin tethers lipid droplets to peroxisomes and directs fatty acid
959 trafficking through ESCRT-III. *J Cell Biol* **218**, 2583-2599 (2019).
960 https://doi.org/10.1083/jcb.201902061
961 61 Fukumoto, J. *et al.* Pivotal roles of Plasmodium falciparum lysophospholipid
962 acyltransferase 1 in cell cycle progression and cytostome internalization. *Commun*
963 *Biol* **8**, 142 (2025). https://doi.org/10.1038/s42003-025-07564-4
964 62 Tougan, T. *et al.* An automated haematology analyzer XN-30 distinguishes
965 developmental stages of falciparum malaria parasite cultured in vitro. *Malar J* **17**, 59
966 (2018). https://doi.org/10.1186/s12936-018-2208-6
967 63 Josling, G. A. *et al.* Dissecting the role of PfAP2-G in malaria gametocytogenesis.
968 *Nature Communications* **11** (2020). https://doi.org/10.1038/s41467-020-15026-0

969 64 Azasi, Y. & Rowe, J. A. Selecting Plasmodium falciparum Infected Erythrocytes for
970 Adhesion to Cell Lines. *Methods Mol Biol* **2470**, 91-100 (2022).
971 https://doi.org/10.1007/978-1-0716-2189-9_9
972 65 Claessens, A. & Rowe, J. A. Selection of Plasmodium falciparum parasites for
973 cytoadhesion to human brain endothelial cells. *J Vis Exp*, e3122 (2012).
974 https://doi.org/10.3791/3122
975 66 Kita, Y., Tokuoka, S. M., Oda, Y. & Shimizu, T. TRACES: A Lightweight Browser for
976 Liquid Chromatography-Multiple Reaction Monitoring-Mass Spectrometry
977 Chromatograms. *Metabolites* **12** (2022). https://doi.org/10.3390/metabo12040354
978 67 Tokuoka, S. M. *et al.* Plasma proteomics and lipidomics facilitate elucidation of the
979 link between Alzheimer's disease development and vessel wall fragility. *Sci Rep* **14**,
980 19901 (2024). https://doi.org/10.1038/s41598-024-71097-9
981

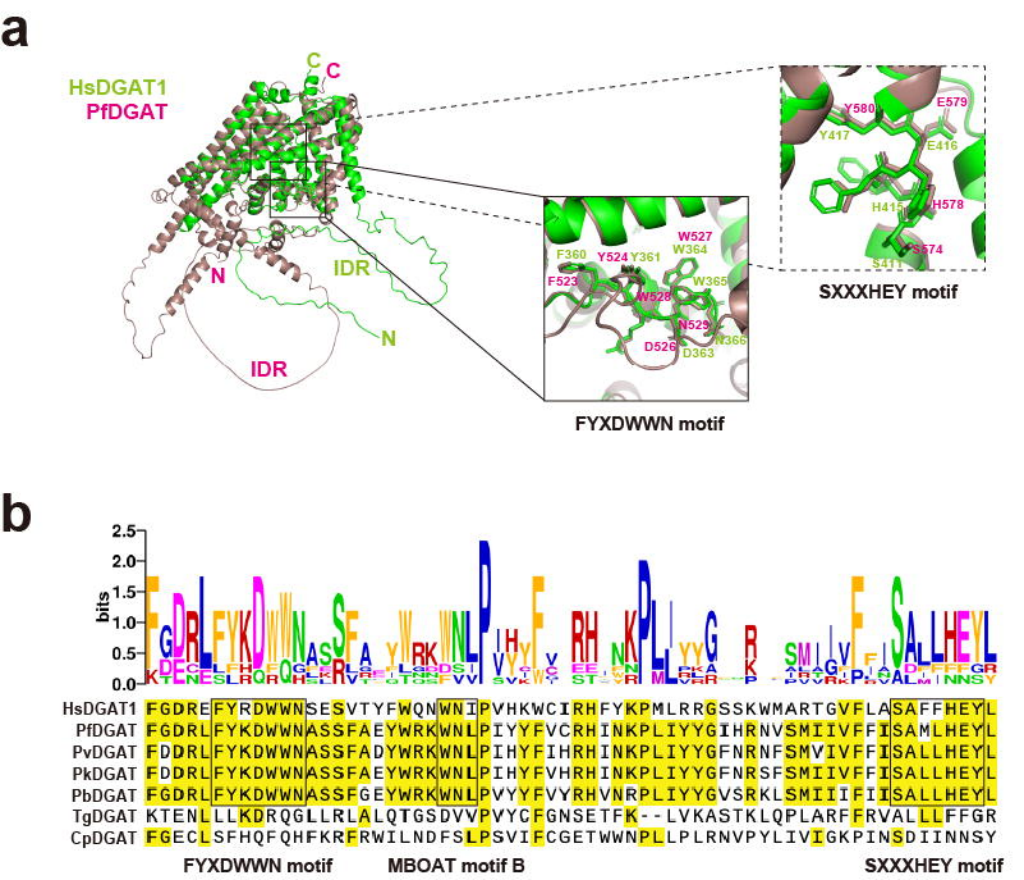
a
HsDGAT1
PfDGAT
C
C
N
IDR
N
IDR
F360
Y524
Y361
W527
W364
F523
W528
W365
N529
D526
D363
W366
FYXDWWN motif
Y580
E579
Y417
E416
H415
H578
S411
S574
SXXXHEY motif
b
bits
2.5
2.0
1.5
1.0
0.5
0.0
HsDGAT1 FGDREFYRDWWNSESVTYFWQNWNIPVHKWCIRHFYKPMLRRGSSKWMARTGVFLASAFFHEYL
PfDGAT FGDRLFYKDWWNASSFAEYWRKWNLPIYYFVCRHINKPLIYYGIHRNVSMIIVFFISAMLHEYL
PvDGAT FDDRLFYKDWWNASSFADYWRKWNLPIHYFIHRHINKPLIYYGFNRNFSMVIVFFISALLHEYL
PkDGAT FDDRLFYKDWWNASSFAEYWRKWNLPIHYFVHRHINKPLIYYGFNRSFSMIIVFFISALLHEYL
PbDGAT FGDRLFYKDWWNASSFGEYWRKWNLPVYYFVYRHVNRPLIYYGVSRKLSMIIIFIISALLHEYL
TgDGAT KTENLLLKDRQGLLRLALQTGSDVVPVYCFGNSETFK--LVKASTKLQPLARFFRVALLLFFGR
CpDGAT FGECLSFHQFQHFKRFRWILNDFSLPSVIFCGETWWNPLLPLRNVPYLIVIGKPINSDIINNSY
FYXDWWN motif
MBOAT motif B
SXXXHEY motif

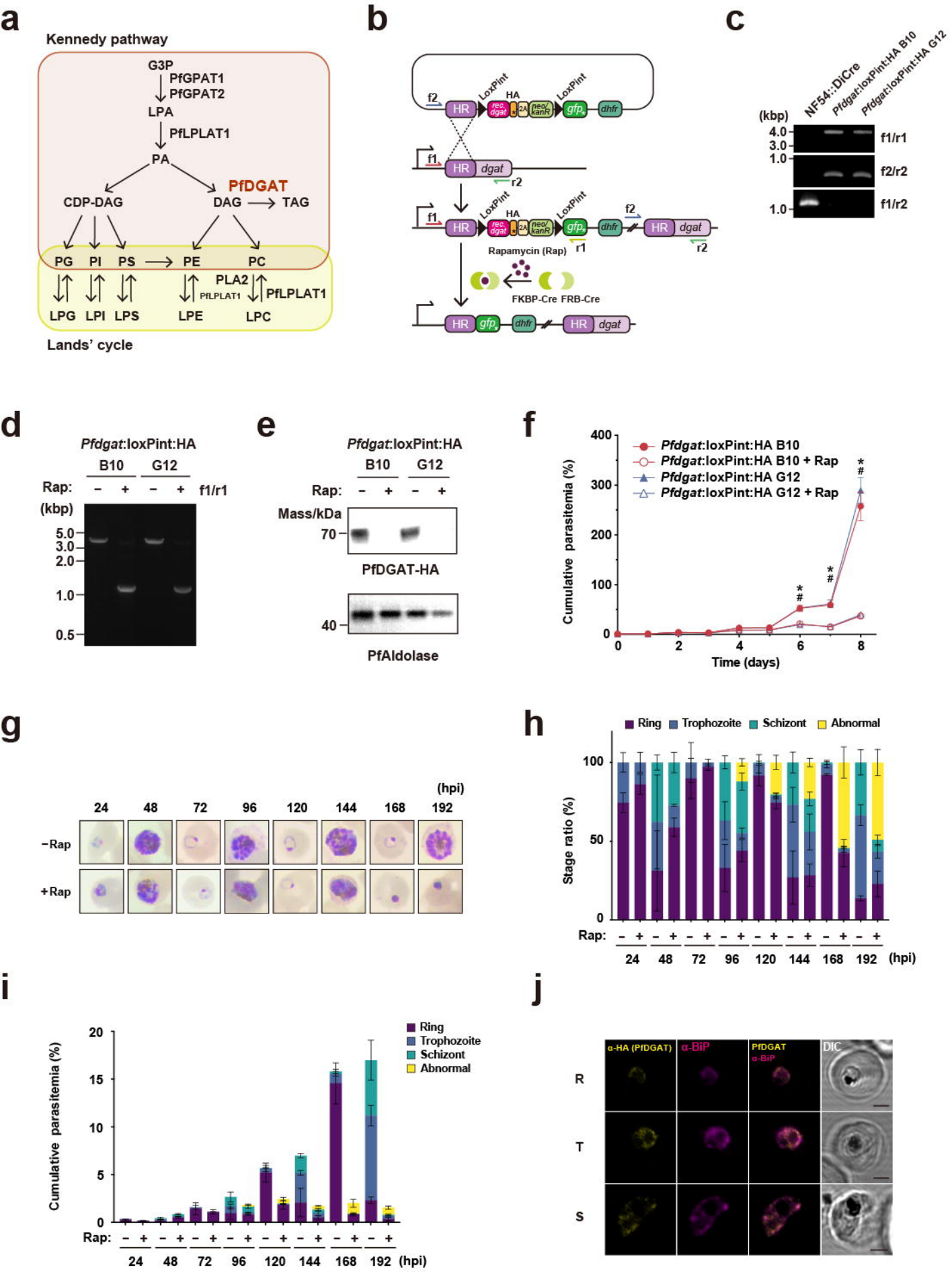
a
Kennedy pathway
G3P
PfGPAT1
PfGPAT2
LPA
PfLPLAT1
PA
PfDGAT
CDP-DAG
DAG
TAG
PG
PI
PS
PE
PC
PLA2
PfLPLAT1
PfLPLAT1
LPG
LPI
LPS
LPE
LPC
Lands' cycle
b
f2
HR
LoxPint
HA
rec. dgat
2A
neo/ kanR
LoxPint
gfp
dhfr
f1
HR
dgat
r2
f1
HR
LoxPint
HA
rec. dgat
2A
neo/ kanR
LoxPint
gfp
dhfr
f2
HR
dgat
Rapamycin (Rap)
r1
r2
FKBP-Cre
FRB-Cre
HR
gfp
dhfr
HR
dgat
c
NF54::DiCre
Pfdgat:loxPint:HA B10
Pfdgat:loxPint:HA G12
(kbp)
4.0
3.0
1.0
f1/r1
f2/r2
1.0
f1/r2
d
Pfdgat:loxPint:HA
B10
G12
Rap:
–
+
–
+
f1/r1
(kbp)
5.0
3.0
2.0
1.0
0.5
e
Pfdgat:loxPint:HA
B10
G12
Rap:
–
+
–
+
Mass/kDa
70
PfDGAT-HA
40
PfAldolase
f
Pfdgat:loxPint:HA B10
Pfdgat:loxPint:HA B10 + Rap
Pfdgat:loxPint:HA G12
Pfdgat:loxPint:HA G12 + Rap
Cumulative parasitemia (%)
400
300
200
100
0
0
2
4
6
8
Time (days)
g
(hpi)
24
48
72
96
120
144
168
192
–Rap
+Rap
h
Ring
Trophozoite
Schizont
Abnormal
Stage ratio (%)
100
50
0
Rap:
24
48
72
96
120
144
168
192
(hpi)
i
Ring
Trophozoite
Schizont
Abnormal
Cumulative parasitemia (%)
20
15
10
5
0
Rap:
24
48
72
96
120
144
168
192
(hpi)
j
α-HA (PfDGAT)
α-BiP
PfDGAT
α-BiP
DIC
R
T
S

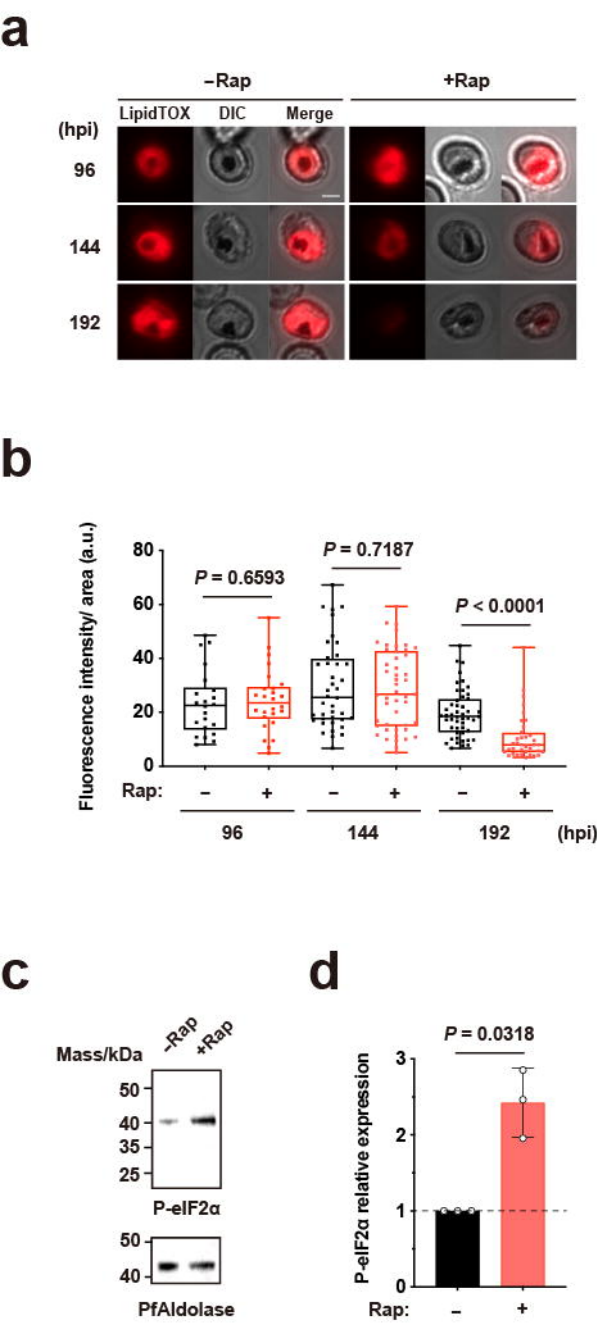
a
−Rap
+Rap
LipidTOX
DIC
Merge
(hpi)
96
144
192
b
Fluorescence intensity/ area (a.u.)
80
60
40
20
0
P = 0.6593
P = 0.7187
P < 0.0001
Rap:
−
+
−
+
−
+
96
144
192
(hpi)
c
Mass/kDa
−Rap
+Rap
50
40
35
25
P-eIF2α
50
40
PfAldolase
d
P = 0.0318
P-eIF2α relative expression
3
2
1
0
Rap:
−
+

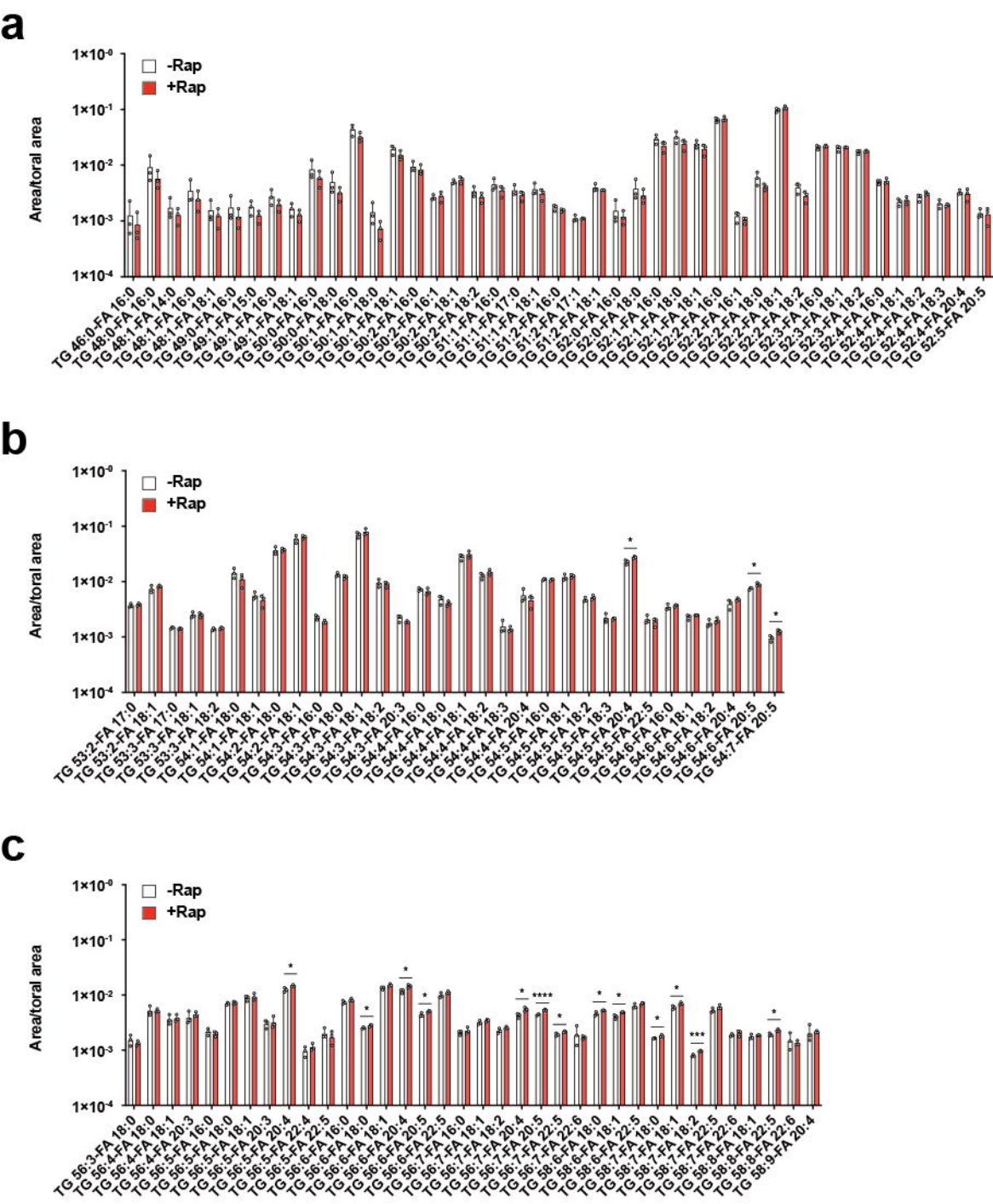
a
-Rap
+Rap
Area/toral area
1×10⁻⁰
1×10⁻¹
1×10⁻²
1×10⁻³
1×10⁻⁴
TG 46:0-FA 16:0
TG 48:0-FA 16:0
TG 48:1-FA 14:0
TG 48:1-FA 16:0
TG 48:1-FA 18:1
TG 49:0-FA 16:0
TG 49:1-FA 15:0
TG 49:1-FA 16:0
TG 49:1-FA 18:1
TG 50:0-FA 16:0
TG 50:0-FA 18:0
TG 50:1-FA 16:0
TG 50:1-FA 18:0
TG 50:1-FA 18:1
TG 50:2-FA 16:0
TG 50:2-FA 16:1
TG 50:2-FA 18:1
TG 50:2-FA 18:2
TG 51:1-FA 16:0
TG 51:1-FA 17:0
TG 51:1-FA 18:1
TG 51:2-FA 16:0
TG 51:2-FA 17:1
TG 51:2-FA 18:1
TG 52:0-FA 16:0
TG 52:0-FA 18:0
TG 52:1-FA 16:0
TG 52:1-FA 18:0
TG 52:1-FA 18:1
TG 52:2-FA 16:0
TG 52:2-FA 16:1
TG 52:2-FA 18:0
TG 52:2-FA 18:1
TG 52:2-FA 18:2
TG 52:3-FA 16:0
TG 52:3-FA 18:1
TG 52:3-FA 18:2
TG 52:4-FA 16:0
TG 52:4-FA 18:1
TG 52:4-FA 18:2
TG 52:4-FA 18:3
TG 52:4-FA 20:4
TG 52:5-FA 20:5
b
-Rap
+Rap
Area/toral area
1×10⁻⁰
1×10⁻¹
1×10⁻²
1×10⁻³
1×10⁻⁴
TG 53:2-FA 17:0
TG 53:2-FA 18:1
TG 53:3-FA 17:0
TG 53:3-FA 18:1
TG 53:3-FA 18:2
TG 54:1-FA 18:0
TG 54:1-FA 18:1
TG 54:2-FA 18:0
TG 54:2-FA 18:1
TG 54:3-FA 16:0
TG 54:3-FA 18:0
TG 54:3-FA 18:1
TG 54:3-FA 18:2
TG 54:3-FA 20:3
TG 54:4-FA 16:0
TG 54:4-FA 18:0
TG 54:4-FA 18:1
TG 54:4-FA 18:2
TG 54:4-FA 18:3
TG 54:4-FA 20:4
TG 54:5-FA 16:0
TG 54:5-FA 18:1
TG 54:5-FA 18:2
TG 54:5-FA 18:3
TG 54:5-FA 20:4
TG 54:5-FA 22:5
TG 54:6-FA 16:0
TG 54:6-FA 18:1
TG 54:6-FA 18:2
TG 54:6-FA 20:4
TG 54:6-FA 20:5
TG 54:7-FA 20:5
c
-Rap
+Rap
Area/toral area
1×10⁻⁰
1×10⁻¹
1×10⁻²
1×10⁻³
1×10⁻⁴
TG 56:3-FA 18:0
TG 56:4-FA 18:0
TG 56:4-FA 18:1
TG 56:4-FA 20:3
TG 56:5-FA 16:0
TG 56:5-FA 18:0
TG 56:5-FA 18:1
TG 56:5-FA 20:3
TG 56:5-FA 20:4
TG 56:5-FA 22:4
TG 56:5-FA 22:5
TG 56:6-FA 16:0
TG 56:6-FA 18:0
TG 56:6-FA 18:1
TG 56:6-FA 20:4
TG 56:6-FA 20:5
TG 56:6-FA 22:5
TG 56:7-FA 16:0
TG 56:7-FA 18:1
TG 56:7-FA 18:2
TG 56:7-FA 20:4
TG 56:7-FA 20:5
TG 56:7-FA 22:5
TG 56:7-FA 22:6
TG 58:6-FA 18:0
TG 58:6-FA 18:1
TG 58:6-FA 22:5
TG 58:7-FA 18:0
TG 58:7-FA 18:1
TG 58:7-FA 18:2
TG 58:7-FA 22:5
TG 58:8-FA 22:6
TG 58:8-FA 18:1
TG 58:8-FA 22:5
TG 58:8-FA 22:6
TG 58:9-FA 20:4

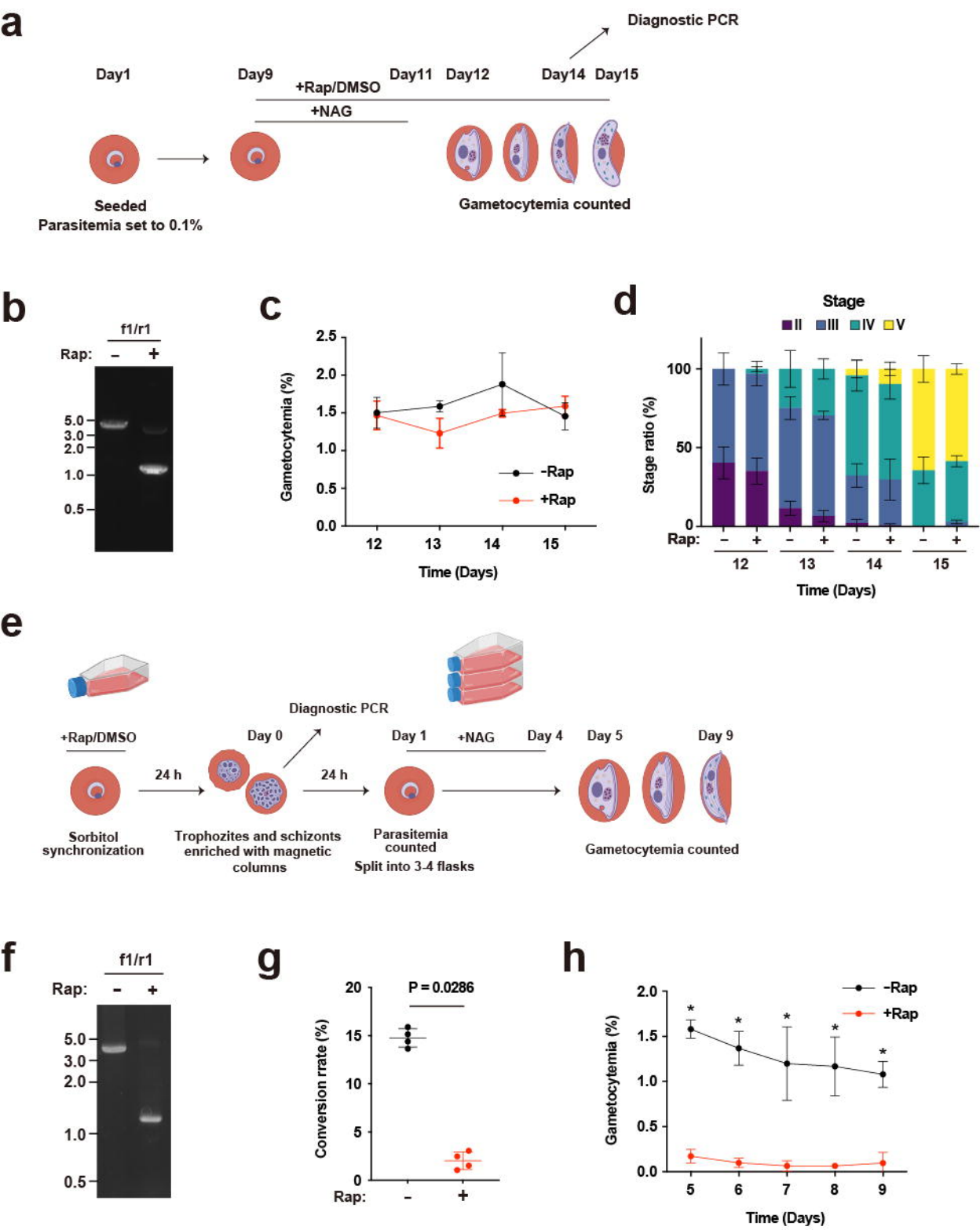
a
Diagnostic PCR
Day1
Day9
Day11
Day12
Day14
Day15
+Rap/DMSO
+NAG
Seeded
Parasitemia set to 0.1%
Gametocytemia counted
b
f1/r1
Rap:
–
+
5.0
3.0
2.0
1.0
0.5
c
Gametocytemia (%)
2.5
2.0
1.5
1.0
0.5
0.0
12
13
14
15
Time (Days)
-Rap
+Rap
d
Stage
II
III
IV
V
Stage ratio (%)
100
50
0
Rap:
–
+
12
13
14
15
Time (Days)
e
Diagnostic PCR
+Rap/DMSO
Day 0
Day 1
+NAG
Day 4
Day 5
Day 9
24 h
24 h
Sorbitol synchronization
Trophozites and schizonts enriched with magnetic columns
Parasitemia counted
Split into 3-4 flasks
Gametocytemia counted
f
f1/r1
Rap:
–
+
5.0
3.0
2.0
1.0
0.5
g
P = 0.0286
Conversion rrate (%)
20
15
10
5
0
Rap:
–
+
h
-Rap
+Rap
Gametocytemia (%)
2.0
1.5
1.0
0.5
0.0
5
6
7
8
9
Time (Days)

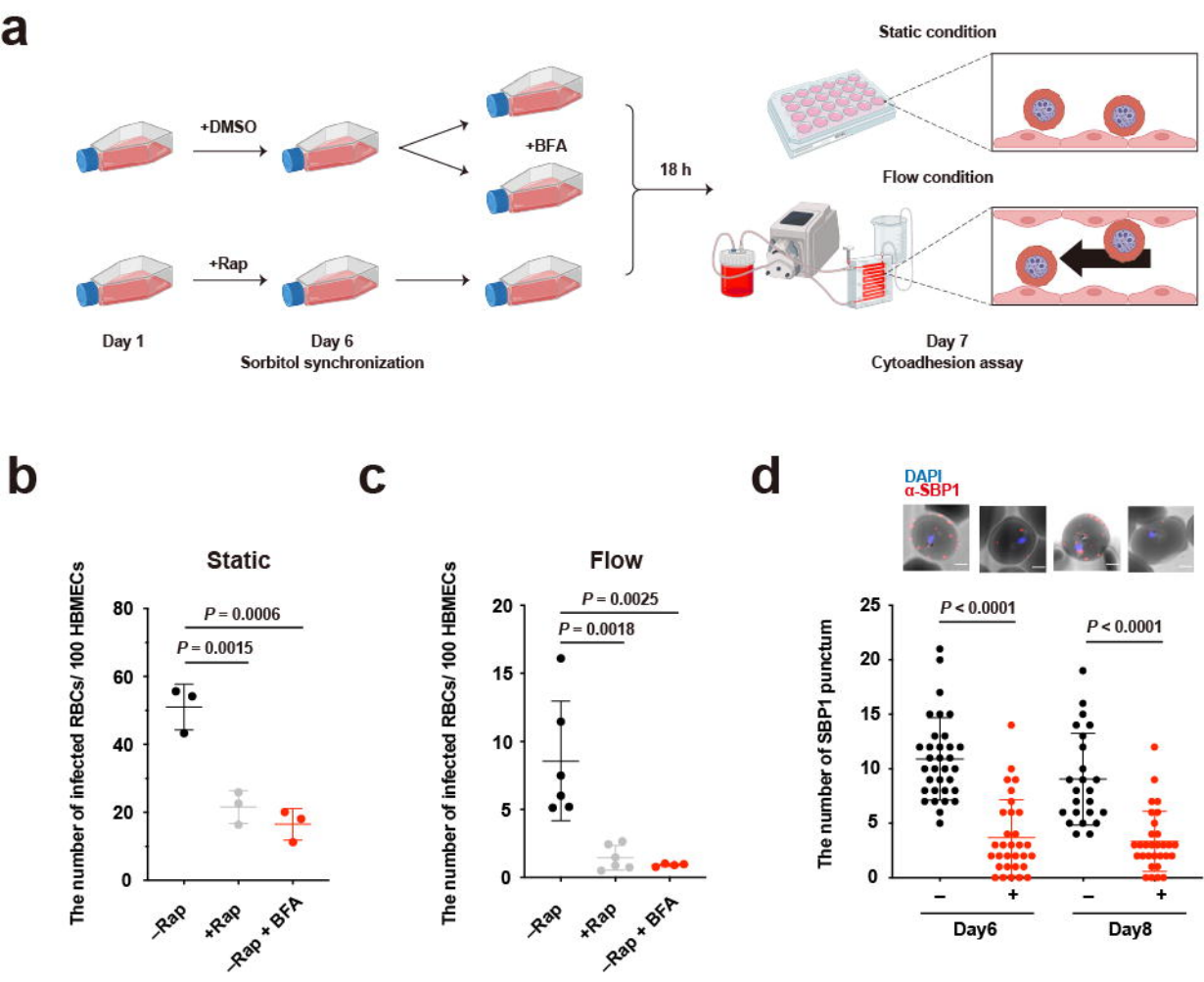
a
+DMSO
+Rap
+BFA
18 h
Static condition
Flow condition
Day 1
Day 6
Sorbitol synchronization
Day 7
Cytoadhesion assay
b
Static
The number of infected RBCs/ 100 HBMECs
P = 0.0006
P = 0.0015
–Rap
+Rap
–Rap + BFA
c
Flow
The number of infected RBCs/ 100 HBMECs
P = 0.0025
P = 0.0018
–Rap
+Rap
–Rap + BFA
d
DAPI
α-SBP1
The number of SBP1 punctum
P < 0.0001
P < 0.0001
Day6
Day8

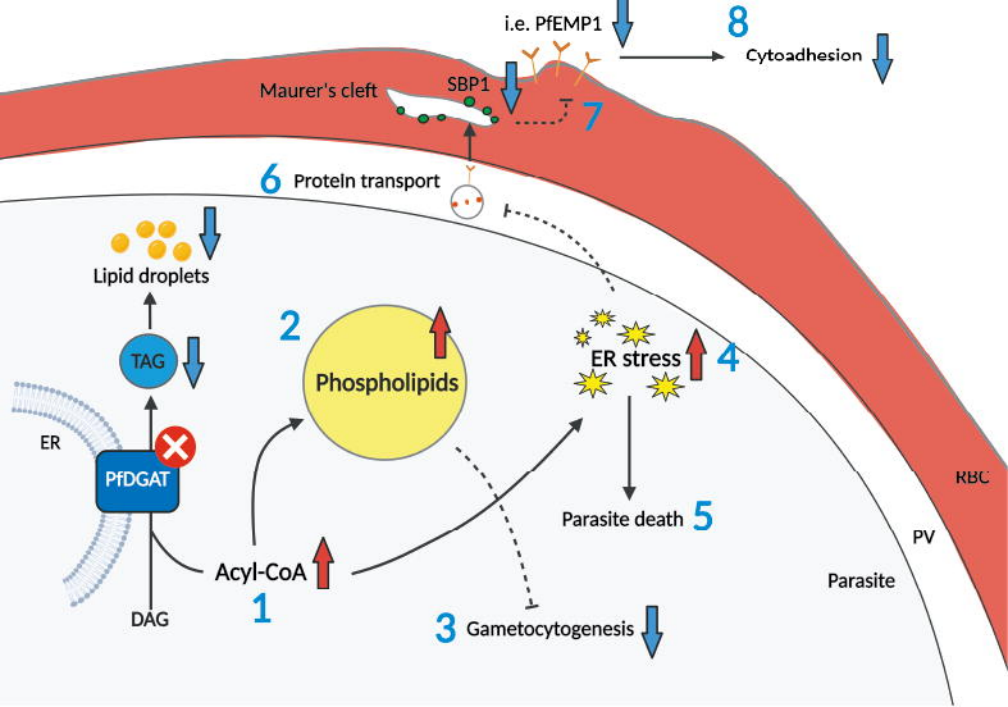
i.e. PfEMP1
8
Cytoadhesion
Maurer's cleft
SBP1
7
6
Proteln transport
Lipid droplets
TAG
2
Phospholipids
ER stress
4
ER
PfDGAT
Parasite death
5
RBC
PV
Parasite
Acyl-CoA
1
DAG
3
Gametocytogenesis